The Company of
Biologists

RESEARCH ARTICLE

ZBTB20 is crucial for the specification of a subset of callosal projection neurons and astrocytes in the mammalian neocortex

Jéssica Alves Medeiros de Araújo[1,2,*], Soraia Barão[1,*], Isabel Mateos-White[3], Ana Espinosa[4], Marcos Romualdo Costa[2,5,‡], Cristina Gil-Sanz[3,‡] and Ulrich Müller[1,‡]

ABSTRACT

Neocortical progenitor cells generate subtypes of excitatory projection neurons in sequential order followed by the generation of astrocytes. The transcription factor zinc finger and BTB domain-containing protein 20 (ZBTB20) has been implicated in regulation of cell specification during neocortical development. Here, we show that ZBTB20 instructs the generation of a subset of callosal projections neurons in cortical layers II/III in mouse. Conditional deletion of *Zbtb20* in cortical progenitors, and to a lesser degree in differentiating neurons, leads to an increase in the number of layer IV neurons at the expense of layer II/III neurons. Astrogliogenesis is also affected in the mutants with an increase in the number of a specific subset of astrocytes expressing GFAP. Astrogliogenesis is more severely disrupted by a ZBTB20 protein containing dominant mutations linked to Primrose syndrome, suggesting that ZBTB20 acts in concert with other ZBTB proteins that were also affected by the dominant-negative protein to instruct astrogliogenesis. Overall, our data suggest that ZBTB20 acts both in progenitors and in postmitotic cells to regulate cell fate specification in the mammalian neocortex.

KEY WORDS: Astrocyte, Callosal neuron, Neocortex, Specification, ZBTB20, Mouse

INTRODUCTION

The generation of cellular diversity in the neocortex requires sequential processes that are orchestrated by genetic and environmental influences (Miller and Gauthier, 2007). Radial glial cells in the ventricular zone (VZ) of the dorsal pallium generate subtypes of glutamatergic projection neurons that settle into neocortical cell layers following an inside-out pattern (Molyneaux et al., 2007). GABAergic neurons are generated from distinct progenitor pools in the ventral pallium (Harwell et al., 2015). Both ventral and dorsal pallium progenitors switch from neurogenesis to gliogenesis at mid-to-late stages of embryonic development, producing astrocytes, oligodendrocytes and ependymal cells (Rowitch and Kriegstein, 2010).

One transcription factor that is implicated in the generation of cellular diversity in the neocortex is zinc finger and BTB domain-containing protein 20 (ZBTB20). Defects in ZBTB20 function are linked to autism spectrum disorder, intellectual disability and agenesis of the corpus callosum (Koul, 2014; Rasmussen et al., 2014; Alby et al., 2018). Alterations in *ZBTB20* have been found in patients with Primrose syndrome, chromosome 3q13.31 microdeletion, microduplication syndromes, and major depressive disorder (Cordeddu et al., 2014; Davies et al., 2014; Koul, 2014; Rasmussen et al., 2014; Mattioli et al., 2016; Mulatinho et al., 2016; Casertano et al., 2017; Jones et al., 2018; Cleaver et al., 2019). Primrose syndrome patients present severe phenotypes, including macrocephaly, intellectual disability and behavioral abnormalities (Cordeddu et al., 2014; Cleaver et al., 2019). Primrose syndrome is an autosomal dominant condition caused by missense mutations that affect the DNA-binding domain of ZBTB20 likely leading to a dominant-negative protein (Cordeddu et al., 2014). However, the mechanisms by which ZBTB20 dysfunction contributes to disease is largely unknown.

ZBTB20 is expressed in the proliferative zone of the developing murine neocortex from embryonic day (E) 15 to E18. During early postnatal ages it is transiently expressed in upper layer cortical projection neurons whereas in the adult its expression is limited to astrocytes (Mitchelmore et al., 2002; Nagao et al., 2016; Tonchev et al., 2016). ZBTB20 overexpression and knockdown by *in utero* electroporation at E15.5 promotes and suppresses astrocytogenesis, respectively (Nagao et al., 2016). In mice with null mutations in *Zbtb20*, numbers of neurons expressing markers for layer IV-VI are increased at early postnatal ages at the expense of neurons expressing markers for layers II/III. It has therefore been proposed that ZBTB20 also regulates the sequential generation of different neuronal subtypes from progenitor cells (Tonchev et al., 2016). However, *Zbtb20* null mice die at early postnatal ages (Rosenthal et al., 2012), thus preventing an analysis of the mature brain, especially astrocytes, which largely develop postnatally (Bandeira et al., 2009; Ge et al., 2012).

To further investigate the function of *Zbtb20* during cortical development, we have generated *Zbtb20-flox* mice. We show here that mice that lack ZBTB20 in cortical progenitors and their offspring live to adulthood. Surprisingly, ZBTB20 has more specific roles in cell fate specification than previously thought. Specifically, ZBTB20 has an instructive role in the generation of a subset of callosal projections neurons (CPNs) and in the development of subtypes of astrocytes. We also provide insights into the effects of a mutation in *Zbtb20* associated with Primrose syndrome on astrocyte development. Overall, our studies reveal specific functions for ZBTB20 in cell type specification in the cortex and suggest that defects in cell type specification likely contribute to some of the symptoms observed in individuals with genetic alterations in *ZBTB20*.

[1]The Solomon H. Snyder Department of Neuroscience, Johns Hopkins University School of Medicine, Baltimore, MD 21205, USA. [2]Brain Institute, Federal University of Rio Grande do Norte, Natal, RN 59056-450, Brazil. [3]BIOTECMED Institute, Universidad de Valencia, Burjassot, Valencia 46100, Spain. [4]AntalGenics, Quorum Building III, Scientific Park - UMH. Avda. de la Universidad, s/n. 03202 Elche (Alicante), Spain. [5]Unité INSERM 1167, RID-AGE-Risk Factors and Molecular Determinants of Aging-Related Diseases, Institut Pasteur de Lille, University of Lille, U1167-Excellence Laboratory LabEx DISTALZ, Lille Cedex 59019, France.
*These authors contributed equally to this work

[‡]Authors for correspondence (mrcosta@neuro.ufrn.br; Cristina.Gil@uv.es; umuelle3@jhmi.edu)

C.G.-S., 0000-0002-7827-5480

DEVELOPMENT

RESULTS

Deletion of *Zbtb20* in cortical progenitors leads to laminar disorganization of the murine neocortex

To study the role of *Zbtb20* in neuronal specification during neocortical development, we generated mice carrying a *Zbtb20-flox* (*Zbtb20^{fl}*) allele. We inactivated *Zbtb20* in neural progenitors starting at E10.5 by crossing *Emx1-Cre/Zbtb20$^{fl/+}$* mice with *Zbtb20$^{fl/fl}$* mice (Fig. 1A) (Gorski et al., 2002). To confirm that *Zbtb20* was inactivated in the dorsal telencephalon, we analyzed ZBTB20 expression by immunohistochemistry of coronal sections at E15.5, given that at earlier time points ZBTB20 was only detected in wild-type mice in the pallial-subpallial boundary (Fig. S1). In control mice, ZBTB20 was detected in PAX6^{+} VZ progenitors, but it was absent in the dorsal telencephalon of *Emx1-Cre;Zbtb20$^{fl/fl}$* animals (referred to as *Zbtb20cKO* mice) (Fig. 1B,C).

We next assessed the expression of neuronal subtype markers in the primary somatosensory cortex (S1) of *Zbtb20cKO* mice by immunohistochemistry: BRN2 (POU3F2; layers II/III, IV; few cells in layer V), RORβ (layer IV), CTIP2 (BCL11B; layers V/VI) and TLE4 (layer VI; few cells in layer V) (Alcamo et al., 2008; Arlotta et al., 2008; Jabaudon et al., 2012; Dominguez et al., 2013; Leone

et al., 2015; Molyneaux et al., 2015). The combination of these markers together with cellular density revealed with DAPI staining allowed us to distinguish the different layers (I: not labeled; II/III: BRN2^{+} only; IV: high levels of RORβ; V: high levels of CTIP2; VI: CTIP2^{+}/TLE4^{+}; Fig. 1D).

In *Zbtb20cKO* mutants at postnatal day (P) 10, the numbers of neurons expressing TLE4 and CTIP2 were unaffected (Fig. 1D,E, individual values and mean; DAPI per/mm^2, mean±s.d.: control 5885±447.4, *Zbtb20cKO* 6288±567.7, P=0.3888, t=0.9659, d.f.=4, n=3 mice per group; CTIP2^{+} cells/mm^2, control 1773±137.9, *Zbtb20cKO* 1990±199.8, P=0.1958, t=1.551, d.f.=4, n=3 mice per group; TLE4^{+} cells/mm^2, control 1464±238.5, *Zbtb20cKO* 1446 ±292.5, P=0.9322, t=0.08950, d.f.=5; n=4 control, n=3 cKO; unpaired *t*-test), but the distribution of deep layer neurons was shifted towards upper positions of the cortex (Fig. 1D). To assess cellular distribution, we divided the cortical plate into ten equivalent bins, with bin 1 corresponding to the deepest and bin 10 corresponding to the most superficial location. Quantification of cells per bin revealed that the distribution of layers V and VI neurons was altered in *Zbtb20cKO* mice (Fig. 1F, mean±s.e.m., Šídák's multiple comparisons test, Table S3), and layers II/III and IV were
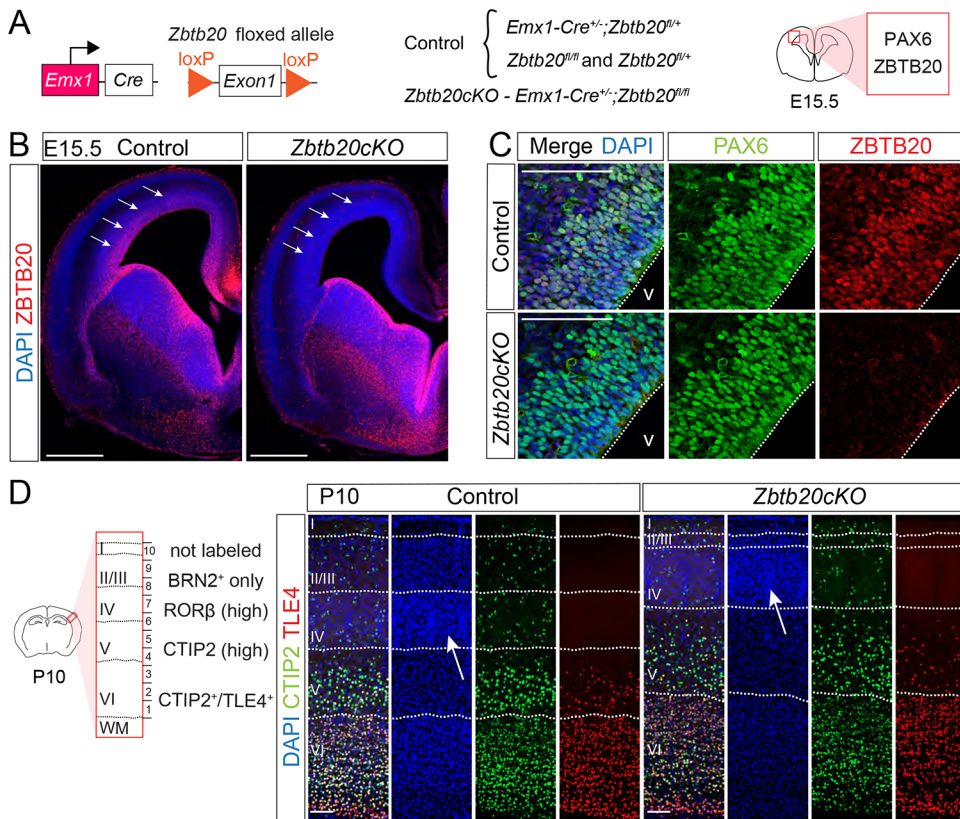

Fig. 1. Genetic inactivation of *Zbtb20* in cortical progenitors does not affect the generation of layer V and VI neurons. (A) Diagram of experimental strategy. *Zbtb20flox* mice were crossed with *Emx1-Cre* mice to inactivate *Zbtb20* in neocortical progenitors. Histological analysis was performed at E15.5. (B,C) Coronal sections of the indicated mice at E15.5 were stained with DAPI and antibodies to ZBTB20 and PAX6. ZBTB20 was absent from the dorsal telencephalon (arrows in B). C shows a higher resolution view of the cortical VZ (V). (D) Coronal sections of the S1 of the indicated mice at P10 stained with DAPI and antibodies to CTIP2 and TLE4. Neocortical cell layers I-VI are indicated. Arrows point to densely packed neurons in controls and mutants (layer IV). Schematic illustrates expression of marker genes. (E) DAPI, CTIP2^{+} and TLE4^{+} cells/mm^2 in S1 are represented as individual values and mean; n=3 mice/ group; unpaired *t*-test; ns, not significant (P≥0.05). (F) DAPI, CTIP2^{+} and TLE4^{+} cellular distribution bins plotted as percentage (mean±s.e.m.; n=3/group; two-way ANOVA; Šídák's multiple comparisons test; **P<0.01; ***P<0.001; ****P<0.0001). Scale bars: 100 μm (C,D); 500 μm (B).
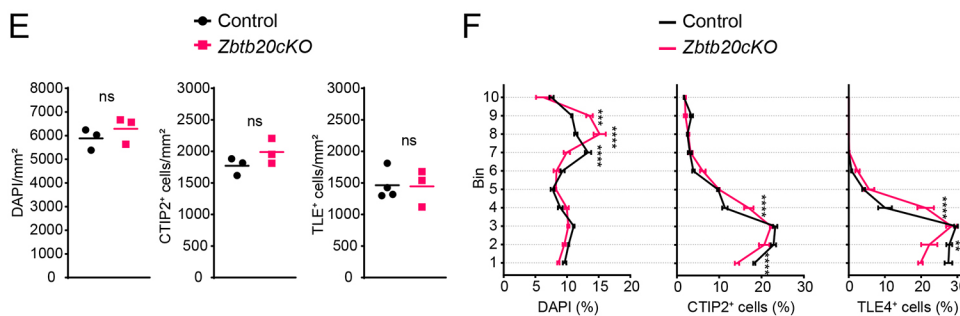
severely disorganized. DAPI staining revealed clusters of densely packed neurons typically found in layer IV now present throughout positions normally occupied by layer II/III neurons (Fig. 1D, arrows; Fig. 2A). Quantification of DAPI-stained nuclei per bin confirmed major disorganization of upper cortical layers (Fig. 1F, mean±s.e.m., Šídák's multiple comparisons test, Table S3). Consistent with the morphological changes, the number of RORβ$^+$ neurons was increased in *Zbtb20cKO* animals at the expense of layer II/III BRN2$^+$ neurons (Fig. 2A, individual values and mean; BRN2$^+$ only cells/mm^2, mean±s.d.: control 556.8 ±29.93, *Zbtb20cKO* 210.2±40.02, *P*=0.0002, t=12.4, d.f.=4; RORβ$^+$ cells/mm^2; control 1865±33.81, *Zbtb20cKO* 2771±285.4, *P*=0.0055, t=5.461, d.f.=4; *n*=3 mice per group; unpaired *t*-test). Some BRN2$^+$ neurons were still detectable, but they were largely found near the top of the reduced layer II/III (Fig. 2C, mean±s.e.m., Šídák's multiple comparisons test, Table S3), suggesting that deletion of ZBTB20 affected the generation of many, but not all, layer II/III neurons. In addition, BRN2$^+$ cells were present in deep

layers of S1 in mutant mice, indicative of neuronal migration defects (Fig. 2B). A similar abnormal distribution of BRN2$^+$ neurons was observed in the anterior cingulate area, motor area, retrosplenial area and cingulum bungle (Fig. 2D).

In agreement with the migration defects, the contribution of neurons to individual neocortical cell layers was affected in *Zbtb20cKO* mice (Fig. 2E,F, individual and mean values), with an increased proportion of NEUN (RBFOX3)$^+$ cells in layers IV and VI, and a reduction of neurons in layer II/III compared with controls (percentage NEUN$^+$ cells, mean±s.d.: layer I, control 1.031±0.1502, *Zbtb20cKO* 1.049±0.2434, *P*>0.9999, t=0.01536; layer II/III, control 19.57±1.429, *Zbtb20cKO* 3.456±0.8575, *P*<0.0001, t=13.95; layer IV, control 27.76±2.141, *Zbtb20cKO* 36.31±1.664, *P*<0.0001, t=7.405; layer V, control 16.71±0.4887, *Zbtb20cKO* 18.94±1.780, *P*=0.2960, t=1.931; layer VI, control 34.93±2.127, *Zbtb20cKO* 40.25 ±1.365, *P*=0.0009, t=4.601; d.f.=20; *n*=3; two-way ANOVA multiple comparisons). However, although the percentage of neurons was reduced in layer II/III and increased in layer IV and
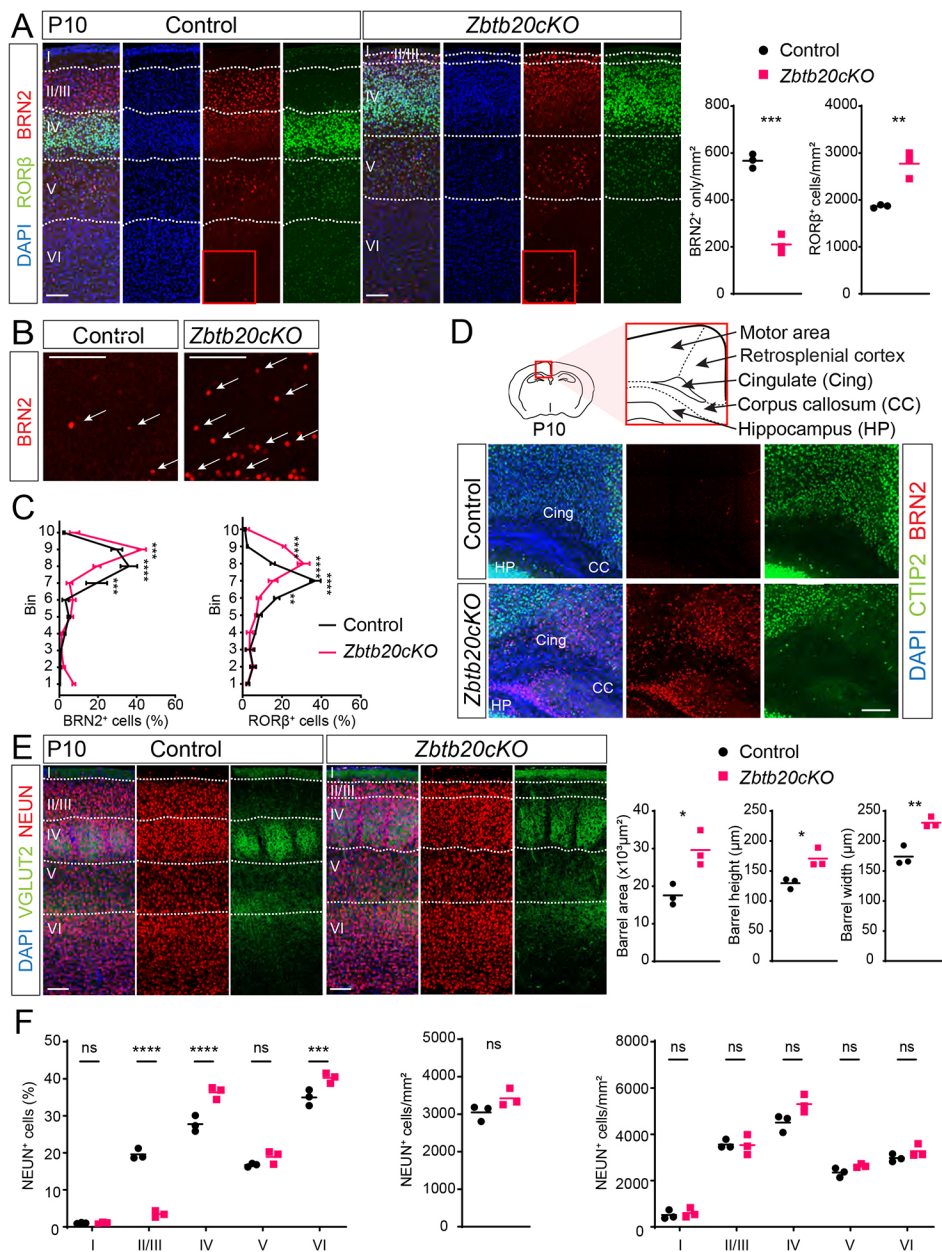

Fig. 2. Genetic inactivation of *Zbtb20* in cortical progenitors leads to defects in the generation of layer II/III neurons and barrel expansion in S1. (A,B) Coronal sections of the S1 of the indicated mice at P10 were stained with DAPI and antibodies to RORβ and BRN2. Red boxes indicate the areas shown in B. Arrows in B point to some BRN2$^+$ neurons in layer VI. Neocortical cell layers I-VI are indicated. In the graphs, BRN2$^+$ only and RORβ$^+$ cells/mm^2 in S1 are plotted as individual values and mean; unpaired *t*-test. (C) BRN2$^+$ and RORβ$^+$ cellular distribution/bins in control and *Zbtb20cKO* mice (percentage cells; mean±s.e.m.; two-way ANOVA; Šídák's multiple comparisons test). (D) Coronal sections of the region indicated in the diagram stained with antibodies to CTIP2 and BRN2. (E) Coronal sections of the S1 of the indicated mice at P10 stained with DAPI and antibodies to NEUN and VGLUT2. Neocortical cell layers I-VI are indicated. The area, height and width occupied by VGLUT2 terminals of thalamic axons are increased in *Zbtb20cKO*; unpaired *t*-test. (F) NEUN$^+$ cells/mm^2 (unpaired *t*-test), cellular density/mm^2 in each layer (multiple unpaired *t*-test, Holm-Šídák method); cellular distribution as percentage (two-way ANOVA, Šídák's multiple comparisons test) represented as individual values and mean. ns, not significant (*P*≥0.05); *P<0.05; **P<0.01; ***P<0.001; ****P<0.0001; *n*=3 mice/group. Scale bars: 100 μm.

VI, the overall cell density of NEUN^{+} cells and DAPI per mm^2 was unaltered in *Zbtb20cKO* cortex (Fig. 2F and Fig. S2 show NEUN and DAPI/mm^2, respectively, individual and mean values, Table S3), along the entire extension of S1 (NEUN^{+} cells/mm^2, mean±s.d.: control 3048±211.1, *Zbtb20cKO* 3423±234.8, P=0.8940, t=2.060, d.f.=4; n=3 mice per group; unpaired t-test) and in each individual layer (NEUN^{+} cells/mm^2, mean±s.d.: layer I, control 514±197.1, *Zbtb20cKO* 599±204.8, P=0.862331, t=0.5224; layer II/III, control 3563±191.5, *Zbtb20cKO* 3533±433.2, P=0.917105, t=0.1108; layer IV, control 4508±374.4, *Zbtb20cKO* 5309±382.8, P=0.268947, t=2.589; layer V, control 2349±202.5, *Zbtb20cKO* 2640±77.79, P=0.284624, t=2.329; layer VI, control 2975±169.2, *Zbtb20cKO* 3273±275.8, P=0.459769, t=1.597; d.f.=4; n=3; multiple unpaired t-tests). The presence of BRN2^{+} ectopic cells in deep layers and normal numbers of CTIP2^{+} and TLE^{+} cells in *Zbtb20cKO* indicate that the expansion of layer VI was due to migration defects of BRN2^{+} cells, although changes in the neuropil could also contribute.

We conclude that ZBTB20 is necessary for the production of normal numbers of layer II/III neurons and their radial migration into S1.

Barrel expansion in S1 of *Zbtb20cKO* mice

In the rodent S1, whiskers are topographically represented as discrete modules of layer IV glutamatergic neurons (barrels) and thalamocortical afferent terminals (Woolsey and Van der Loos, 1970; O'Leary et al., 1994). Because the number of RORβ[+] layer IV neurons was increased in *Zbtb20cKO* mice, we wondered whether the formation of somatosensory circuits might be affected. We stained coronal sections of thalamocortical axons targeting the S1 area with antibodies to the vesicular glutamate transporter 2 (VGLUT2; SLC17A6) (Fig. 2E). In contrast to controls, barrels in *Zbtb20cKO* mice were increased in size: the area, height and width occupied by VGLUT2 terminals of thalamic axons were significantly increased (Fig. 2E, individual values and mean; barrel area in ×10^3 μm^2, mean±s.d.: control 17.553±2.797, *Zbtb20cKO* 29.619±4.728, P=0.0190, t=3.805, d.f.=4; barrel height in μm; control 129.7±8.826, *Zbtb20cKO* 170.6±15.89, P=0.0176, t=3.897, d.f.=4; barrel width in μm; control 174.0±16.18, *Zbtb20cKO* 230.5±8.825, P=0.0060, t=5.312, d.f.=4; n=3 mice per group; unpaired t-test).

Zbtb20 overexpression at mid-neurogenesis leads to premature generation of neurons expressing molecular markers for CPNs

Layer IV neurons are born in mice in large numbers at E14.5, prior to the generation of layer II/III neurons (Telley et al., 2019). To determine whether forced overexpression of ZBTB20 in the VZ at E14.5 instructs progenitors to generate neurons with properties of layer II/III neurons at the expense of layer IV neurons, we carried out *in utero* electroporations. To track electroporated cells, we performed the experiments in Ai9 mice, which contain a Cre-inducible td-Tomato transgene (Madisen et al., 2010). The mice were electroporated either with a control plasmid expressing GFP and Cre (pCAG-GFP-IRES-Cre, referred to as Control) or expressing *Zbtb20* and Cre (pCAG-Zbtb20-IRES-Cre, referred to as *Zbtb20*^{WT}). The laminar position and molecular phenotype of electroporated cells was evaluated postnatally (Fig. 3A).

ZBTB20 was expressed in progenitors at E14.5 that had been electroporated 10 h beforehand with *Zbtb20*^{WT} plasmid, with no detectable expression in control embryos electroporated with Control plasmid (Fig. 3B). In controls, offspring of the electroporated progenitors expressing BRN2 and RORβ and were distributed at P10 throughout layers II/III and IV (Fig. 3C).

Offspring of progenitors electroporated to express ZBTB20^{WT} were predominantly localized in layer II/III and expressed BRN2 but not RORβ (Fig. 3C).

At P22, when neuronal migration and differentiation were largely complete, we observed no differences in the number of NEUN^{+} neurons in the neocortex of mice electroporated to express *Zbtb20*^{WT} (Fig. S3, individual and mean; percentage of NEUN[+]tdTomato^{+} cells, mean±s.d.: Control 59.17±12.33, *Zbtb20*^{WT} 68.06±6.999; P=0.2562, t=1.255, d.f.=6; n=4 mice per group; unpaired t-test). Similarly to what we found at P10, electroporated neurons in controls were distributed throughout layers II/III and IV, whereas cells electroporated to express ZBTB20 were largely confined to layers II/III (Fig. 3D,E, individual values and mean; percentage of tdTomato^{+} neurons in layers II/III, mean±s.d.: Control 55.72±13.08, *Zbtb20*^{WT} 98.53±0.8050, P<0.0001, t=6.552, d.f.=12; percentage of tdTomato^{+} neurons in layers IV, Control 43.86±13, *Zbtb20*^{WT} 0.9256±0.8724, P<0.0001, t=6.57, d.f.=12; n=4 mice per group; two-way ANOVA multiple comparisons).

We conclude that ZBTB20 expression instructs E14.5 progenitors to generate neurons expressing layer II/III markers at the expense of neurons expressing layer IV markers.

Interhemispheric connections of layer II/III CPNs are compromised in *Zbtb20cKO* mice

To evaluate further the phenotypic changes in *Zbtb20cKO* mice, we analyzed the morphological features of CPNs. In wild-type mice, the cell bodies of CPNs reside predominantly in layer II/III with lower numbers in layer IV-VI (Ivy and Killackey, 1982; Catapano et al., 2001; MacDonald et al., 2018). We anticipated that the number of CPNs and their projections would be altered in *Zbtb20cKO* mice owing to the increase in the number of neurons expressing layer IV markers (RORβ[+]), and decrease in the number of neurons expressing layer II/III markers (BRN2^{+}). However, significant numbers of neurons expressing layer II/III markers remained in the mutants, especially in the outer region normally occupied by layer II/III neurons (Fig. 2A), suggesting that layer II/III CPNs are present in the mutants, albeit in reduced numbers.

To identify axonal projections, we labeled CPNs of the somatosensory cortex in control and *Zbtb20cKO* mice by *in utero* electroporation at E15.5, coincident with the generation of layer II/III neurons in wild type, using plasmid vectors expressing RFP or YPET (pCAG-RFP or pCAG-YPET) (Fig. 4A). We carried out histological analysis of the electroporated brains between P10 (Fig. 4A-F) and P13 (Fig. 5A-C) because callosal axons cross the midline and arborize in the somatosensory cortex during the second postnatal week (Wise and Jones, 1978; Ivy and Killackey, 1982).

In controls and *Zbtb20cKO* mice, neurons generated from progenitors electroporated at E15.5 were largely located above layer V neurons and formed normal layers II-IV in wild-type mice and a compressed layer II/III in *Zbtb20cKO* mice (Fig. 4C). No significant difference was observed in the number of electroporated RFP^{+} neurons in *Zbtb20cKO* mice compared with controls (Fig. 4C, individual values and mean; RFP^{+} neurons/mm^2, mean±s.d.: control 294.8±75.06, *Zbtb20cKO* 310.8±51.57, P=0.6263, t=0.4978, d.f.=14; n=8; unpaired t-test). RFP[+] axonal projections forming the corpus callosum (CC) were present in controls and *Zbtb20cKO* mice, with no significant difference in the RFP fluorescence intensity in the CC [Fig. 4B,D, individual values and mean; RFP fluorescence intensity in arbitrary units (a.u.), mean±s.d.: control 51.79±11.75, *Zbtb20cKO* 51.49±10.22; P=0.7221, t=0.05442, d.f.=14; n=8; unpaired t-test]. Higher resolution images of the contralateral, non-electroporated cortical hemisphere revealed
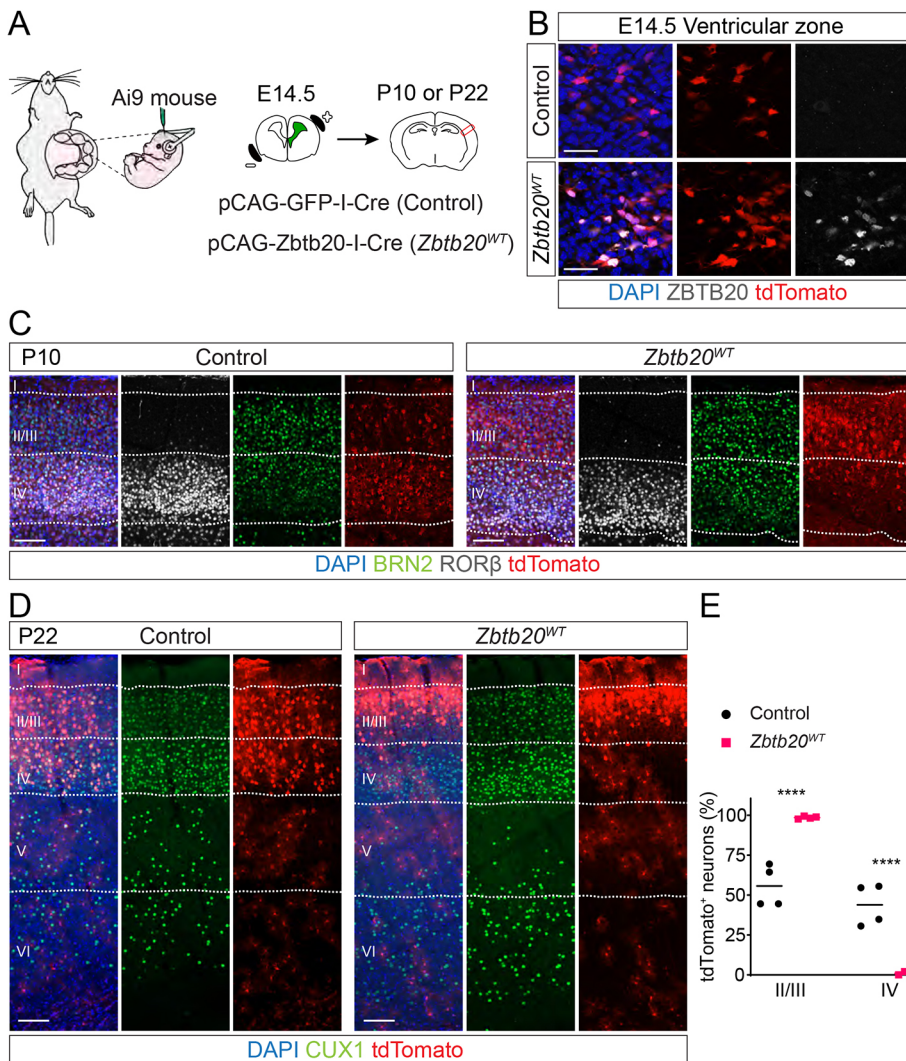
Fig. 3. Overexpression of ZBTB20 in cortical progenitors at E14.5 induces the formation of layer II/III neurons. (A) Schematic of the experimental strategy. *In utero* electroporation was carried out in Ai9 mice at E14.5 with the indicated plasmids. Histological analysis was performed at P10 and P22. (B) Coronal sections of the VZ of electroporated mice at E14.5 stained with DAPI and antibody to ZBTB20. tdTomato detected by its intrinsic fluorescence. (C) Coronal sections of S1 of the indicated mice at P10 (C) and P22 (D) were stained with DAPI and antibodies to BRN2 and RORβ (C) or CUX1 (D). Neocortical cell layers I-VI are indicated. I, IRES; p, promoter; WT, wild type. (E) Percentage tdTomato^{+} neurons in layers II/III and IV represented as individual values and mean; *n*=4 mice/group; two-way ANOVA; ****P<0.0001. Scale bars: 30 μm (B); 100 μm (C,D).

that callosal projections in controls invaded layers II/III of the somatosensory cortex. In contrast, fewer axons of electroporated *Zbtb20cKO* neurons reached the somatosensory cortex and even fewer reached layers II/III (Fig. 4E) (fluorescence intensity for RFP from the white matter to the pial surface in a.u.; mean±s.d.: control 6.677±0.68, *Zbtb20cKO* 3.715±0.669; *n*=5 mice per group; Kolmogorov–Smirnov test; *P*<0.0001).

Some axons in *Zbtb20cKO* mice crossing the midline appeared disorganized, forming aberrant axonal bundles within the ipsilateral cortex (Fig. 4F, white arrowheads), and abnormally targeted the hippocampus (Fig. 4F, unfilled arrowheads). To confirm these observations, we conducted immunohistochemistry against neurofilament at P45 (Fig. 4G) and L1CAM (L1) at P10 and P45 (Fig. S4), which label most of the cortical axon tracts in the postnatal brain. Axons forming the CC in *Zbtb20cKO* mice seemed to defasciculate prior to reaching the midline (Fig. 4G, yellow arrowheads), abnormally targeted the hippocampus (Fig. 4G, open arrowhead), and formed aberrant axonal bundles within the ipsilateral cortex (Fig. 4G, white arrowheads). Surprisingly, we found no differences in CC thickness at the midline at P10 (Fig. S4A, individual values and mean; CC thickness at midline as percentage of control, mean±s.d.: control 98.60±16.82, *Zbtb20cKO* 108.2±19.84; *P*=0.4331, t=0.8253, d.f.=8; *n*=5 per group; unpaired *t*-test) and P45 (Fig. S4B, individual values and

mean; CC thickness at midline as percentage of control, mean±s.d.: control 100.0±9.644, *Zbtb20cKO* 93.67±4.726; *P*=0.3648, t=1.021, d.f.=4; *n*=3 per group; unpaired *t*-test). These findings suggest that layer II/III CPNs in *Zbtb20cKO* mice have lost their normal properties, forming aberrant projections, but that substantial numbers of neurons still form callosal projections indicating that not all neurons are completely re-specified.

Layer V and layer VI appeared unaffected in *Zbtb20cKO* mice (Fig. 1D). To address whether CPNs in deep cortical layers that were generated before E15.5 formed normal axonal projections across the CC in mutants, we carried out *in utero* electroporation of pCAG-YPET at E13.5 and analyzed histological sections at P13 (Fig. 5A). Consistent with the known birth date of neurons generated from progenitor cells at E13.5 (Telley et al., 2019), cell bodies of electroporated cells in wild-type and *Zbtb20cKO* mice were located in deep layers and the lower part of layer IV at P13 (Fig. 5B). YPET[+] axons in controls and mutants projected to and branched within layer V of the contralateral hemisphere (Fig. 5C).

To determine the contribution of all CPNs to the formation of the CC, we injected retrobeads into S1 at P30 to retrogradely trace cortical axons (Fig. 5D,E). Brains were sectioned at P36 and stained with layer markers (Fig. 5F). The number of retrobeads in upper layers neurons was dramatically reduced in *Zbtb20cKO* mice (Fig. 5G, mean±s.e.m.; percentage retrobead^{+} cells/total, mean
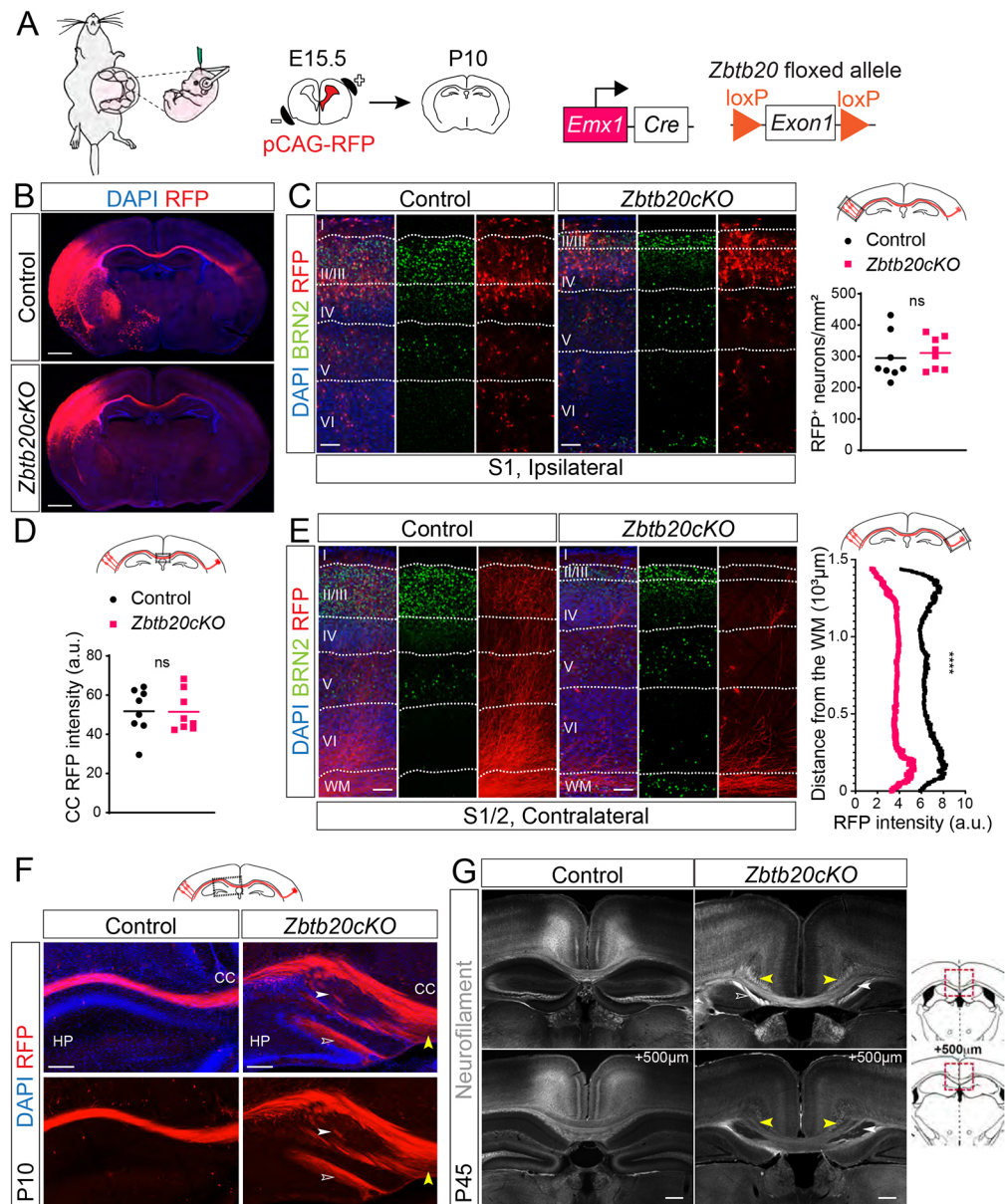
Fig. 4. Callosal projections of layer II/III neurons are affected in *Zbtb20cKO* mice. (A) Schematic of the experimental strategy. *In utero* electroporation with pCAG-RFP at E15.5 in *Zbtb20cKO* mice and controls, histological sections analyzed at P10. (B) Coronal sections of the indicated mice stained with DAPI after electroporation with pCAG-RFP. (C) Coronal sections of the electroporated (ipsilateral) hemisphere of the S1 stained with DAPI and an antibody to BRN2. The number of RFP$^+$ neurons/mm^2 is represented as individual values and mean; n=8 mice/group; unpaired t-test. (D) RFP fluorescence intensity in the middle of the CC represented as arbitrary units (a.u.), individual values and mean; n=8 mice/group; unpaired t-test. (E) Coronal sections of the non-electroporated (contralateral) hemisphere of S1/2 stained with DAPI and an antibody to BRN2. RFP fluorescence intensity plotted from the white matter (WM) to the pial surface (data represented as mean; n=5 mice/group; Kolmogorov–Smirnov test; ****P<0.0001). RFP was detected by its intrinsic fluorescence. (F) Coronal sections of the hippocampus stained with DAPI after electroporation with pCAG-RFP at P10. Note disorganization of the CC axons crossing the midline (yellow arrowheads), aberrant axonal bundles on the ipsilateral cortex (white arrowheads), and axons abnormally targeting the hippocampus (unfilled arrowheads) in *Zbtb20cKO* mice. (G) Coronal sections of the two indicated rostrocaudal levels at P45 stained with antibody to neurofilament. Note axons forming the CC in *Zbtb20cKO* mice seemed to defasciculate prior reaching the midline (yellow arrowheads), abnormally targeted the hippocampus (unfilled arrowhead), and formed aberrant axonal bundles within the ipsilateral cortex (white arrowheads). ns, not significant (P≥0.05). Schematics above graphs indicate the regions examined. Scale bars: 100 μm (C,E); 200 μm (F,G); 1000 μm (B).

±s.d.: bin 10 control 8.806, *Zbtb20cKO* 0.9605, P=0.0095, t= 3.418, d.f.=90; bin 9 control 17.05, *Zbtb20cKO* 1.84, P<0.0001, t= 6.627, d.f.=90; Šídák's multiple comparisons test; n=5 control and n=4 cKO). This observation was confirmed by retrobead$^+$ cells expressing CUX1 (percentage retrobead$^+$CUX1$^+$ cells/total, mean ±s.d.: bin 10 control 21.06, *Zbtb20cKO* 2.862, P=0.0063, t=3.54, d.f.=90; bin 9 control 45.43, *Zbtb20cKO* 4.283, P<0.0001, t=8.005,

d.f.=90; Šídák's multiple comparisons test). We also observed an increased number of retrobead$^+$ cells expressing CUX1 in the deep layers of the cortex in mutants (percentage retrobead$^+$CUX1$^+$ cells/ total, mean±s.d.: bin 2 control 0.9923, *Zbtb20cKO* 30.85, P<0.0001, t=5.81, d.f.=90; bin 1 control 0.2347, *Zbtb20cKO* 17.8, P=0.0095, t=3.418, d.f.=90; Šídák's multiple comparisons test), consistent with the presence of BRN2$^+$ cells in the deep layers
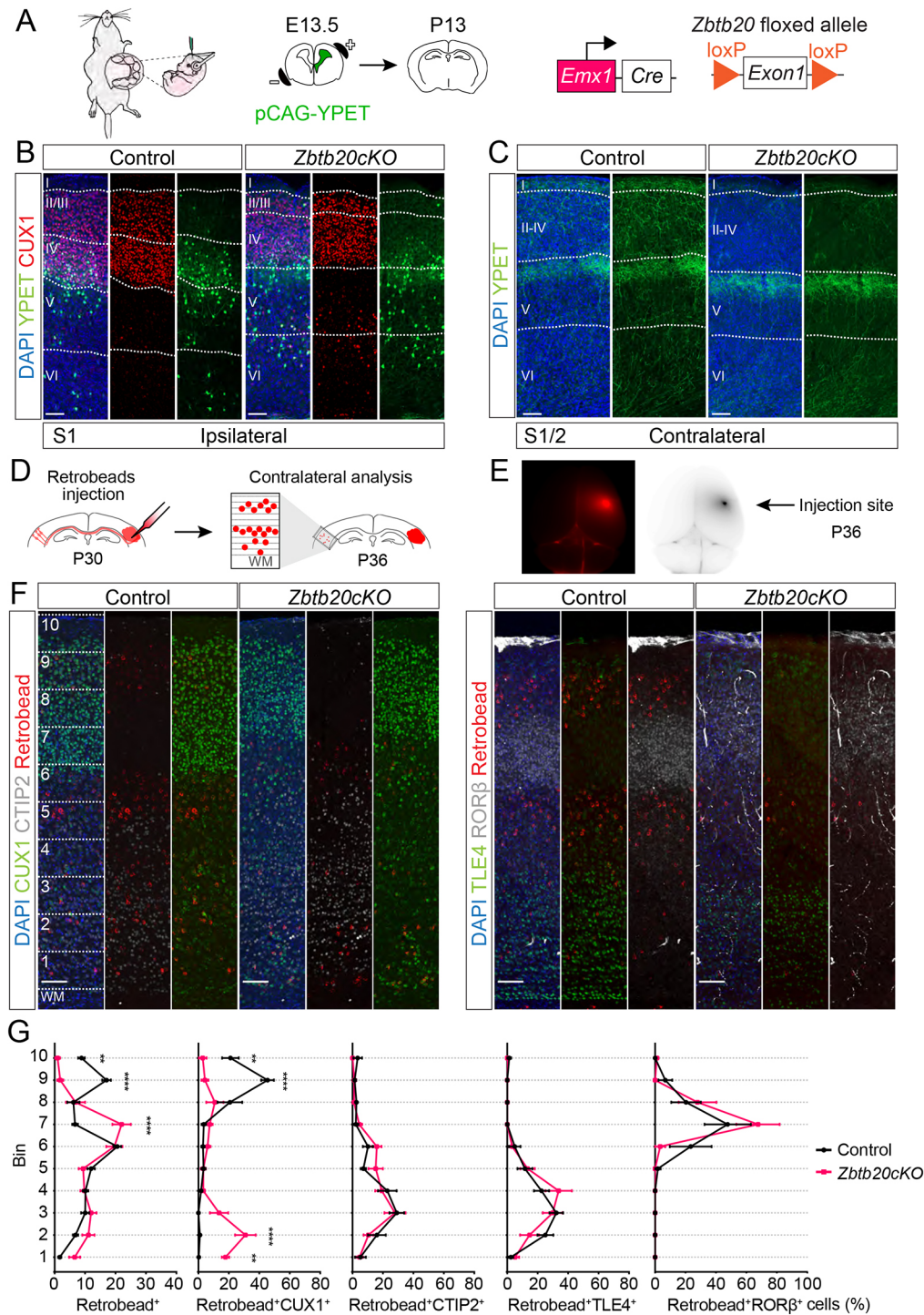
Fig. 5. Callosal projections of deep layer neurons to contralateral deep layers are not affected in *Zbtb20cKO* mice. (A) Schematic of experimental strategy. *In utero* electroporation carried out with pCAG-YPET at E13.5, histological sections analyzed at P13. (B) Coronal sections of the electroporated (ipsilateral) hemisphere of S1 stained with DAPI and an antibody to CUX1. (C) Coronal sections of the non-electroporated (contralateral) hemisphere of S1/S2 stained with DAPI. YPET detected by its intrinsic fluorescence. (D) Schematic of experimental strategy. Retrobeads were injected into S1 at P30 to retrogradely trace axons in the contralateral hemisphere. Analysis was carried out at P36 (E,F). (E) Representative image of the injection site shown in red and black and white contrast at P36. (F) Coronal sections counterstained with CUX1, CTIP2 and DAPI (left panels) or RORβ, TLE4 and DAPI (right panels) to assess the laminar position of the callosal projection neurons. The cortical plate was divided into ten bins, from the border of the white matter with layer VI (bin 1) to the pial surface (bin 10). (G) Percentage of retrobeads in each bin plotted as mean±s.e.m. **$P<0.01$; ****$P<0.0001$; two-way ANOVA (Šídák's multiple comparisons test; $n=6$ control and $n=5$ cKO). Scale bars: 100 μm.

of the cortex (Fig. 2A,B). Additionally, we observed an increased proportion of retrobead^{+} cells in bin 7 in *Zbtb20cKO* mice (percentage retrobead^{+} cells/total, mean±s.d.: bin 7 control 6.712, *Zbtb20cKO* 22, $P<0.0001$, t=6.659, d.f.=90; Šídák's multiple comparisons test). As we did not observe differences in the expression of molecular markers in neurons occupying bin 7, this most likely corresponded to the shift in the distribution of deep layer neurons towards upper layers (Fig. 1). We also found no differences in the number of retrobead^{+} cells expressing RORβ, CTIP2 or TLE4, corresponding to layers IV, V and VI, respectively (Table S3).

These findings suggest that ZBTB20 is crucial for the normal generation and differentiation of layer II/III CPNs, but not for CPNs found in deep neocortical cell layers.

Deletion of *Zbtb20* in postmitotic neurons impairs CPN differentiation

ZBTB20 is expressed transiently in a subset of BRN2^{+} neurons in layer II/III (Tonchev et al., 2016). Thus, defects in *Zbtb20cKO* mice could be explained by the absence of ZBTB20 in post-mitotic neurons. To address this possibility directly, we knocked out *Zbtb20* using *Nex-Cre* mice that express Cre in newly generated
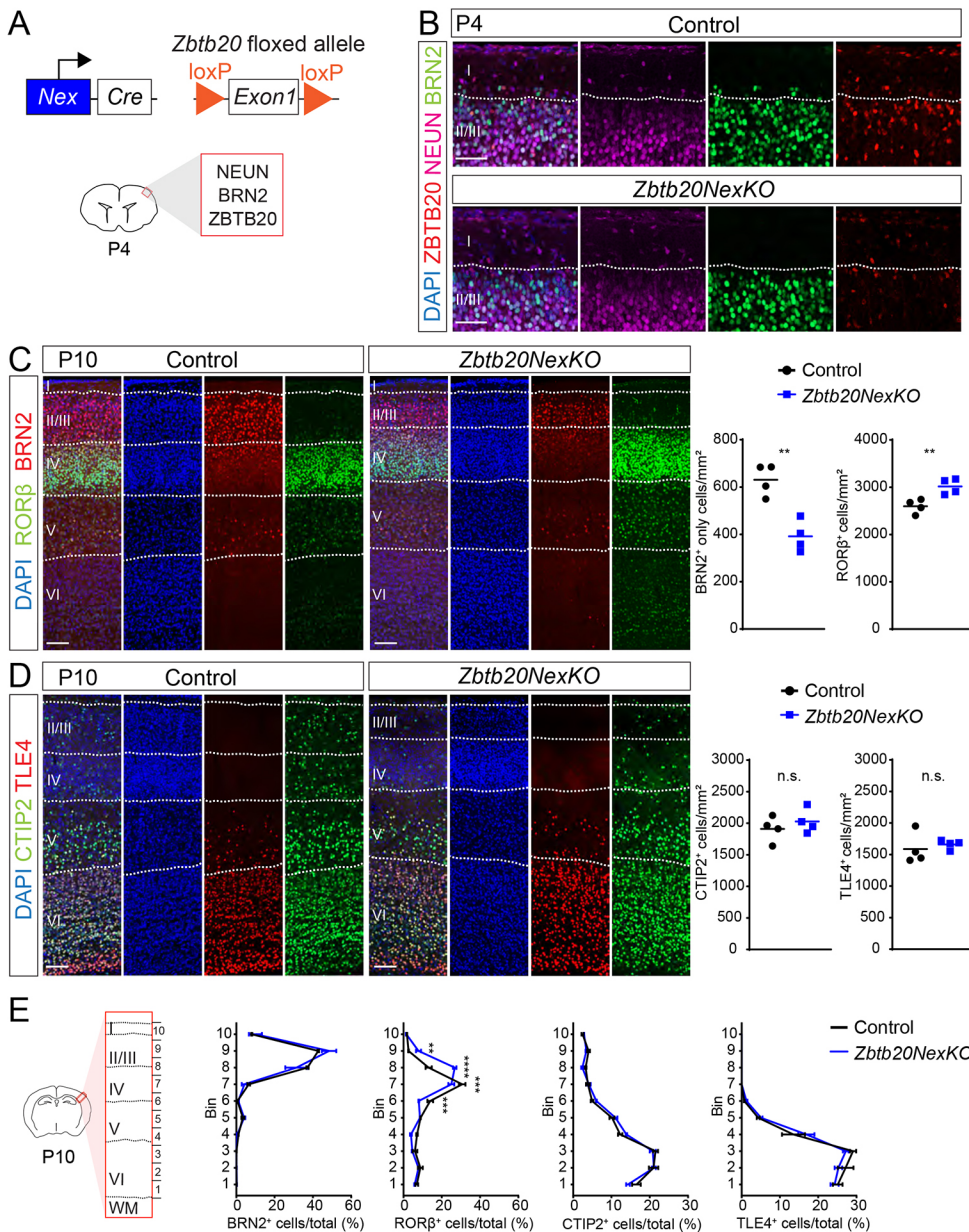
DEVELOPMENT

Fig. 6. Genetic inactivation of *Zbtb20* in newborn cortical neurons leads to defects in the generation of layer II/III neurons. (A) Schematic of experimental strategy. *Zbtb20flox* mice crossed with *Nex-Cre* mice to inactivate *Zbtb20* in newborn cortical neurons. Histological analysis was performed at P4 and P10. (B) Coronal sections of S1 at P4 stained with DAPI and antibodies to ZBTB20, NEUN and BRN2. (C,D) Coronal sections of the S1 at P10 stained with DAPI and antibodies to RORβ and BRN2 (C) or CTIP2 and TLE4 (D). Data are represented as individual values and mean; *n*=4 mice/group; unpaired *t*-test. (E) Schematic showing the analyzed region, with S1 divided into ten longitudinal bins at P10. BRN2^{+}, RORβ[+], CTIP2^{+} and TLE4^{+} cellular distribution/bins plotted as percentage, mean±s.e.m.; *n*=4/group; two-way ANOVA; Šídák's multiple comparisons test. n.s., not significant (*P*≥0.05); **P*<0.01; ***P*<0.001; ****P*<0.0001. Scale bars: 50 μm (B); 100 μm (C,D).

glutamatergic neurons of the dorsal telencephalon (Fig. 6A) (Wu et al., 2005; Goebbels et al., 2006; Belvindrah et al., 2007). Mutant mice will be referred to as *Zbtb20NexKO* mice. Immunohistochemistry at P4 confirmed that in controls ZBTB20 was present in a subset of BRN2^{+} neurons, but it was nearly absent in cortical neurons of *Zbtb20NexKO* mice (Fig. 6B). Numbers of BRN2^{+} only (layer II/III) neurons were reduced in *Zbtb20NexKO* mice compared with controls (Fig. 6C, BRN2^{+} only cells/mm^2, mean±s.d.: control 630.8±66.04, *Zbtb20NexKO* 391.8±65.46, *P*=0.0021, t=5.140, d.f.=6; *n*=4 mice per group; unpaired *t*-test), whereas numbers of RORβ^{+} neurons were increased (Fig. 6C, RORβ^{+} cells/mm^2, mean±s.d.: control 2598±149.5, *Zbtb20NexKO* 3016±164.1, *P*=0.0093, t=3.769, d.f.=6; *n*=4 mice per group; unpaired *t*-test). No change was observed in the number of CTIP2^{+} and TLE4^{+} neurons in *Zbtb20NexKO* mice (Fig. 6D, CTIP2^{+} cells/mm^2, mean±s.d.: control 1910±201.0, *Zbtb20NexKO* 2029±193.9; *P*=0.4288, t=0.8483, d.f.=6, *n*=4 mice per group; TLE4^{+} cells/mm^2, mean±s.d.: control 1587±249.7, *Zbtb20NexKO*

1661±74.20; *P*=0.5940, t=0.5627, d.f.=6; *n*=3 mice per group; unpaired *t*-test).

In accordance with these data, the number of NEUN^{+} cells in *Zbtb20NexKO* was increased in layer IV and reduced in layer II/III; layers I, V and VI were not affected (Fig. S5, percentage NEUN^{+} cells, mean±s.d.: layer I, control 0.8181±0.1430, *Zbtb20NexKO* 1.396±0.3534, *P*=0.9744, t=0.6519; layer II/III, control 20.57±0.7439, *Zbtb20NexKO* 14.47±1.705, *P*<0.0001, t=6.889; layer IV, control 24.74±0.5042, *Zbtb20NexKO* 27.62±0.9352, *P*=0.0142, t=3.247; layer V, control 17.78±1.793, *Zbtb20NexKO* 18.09±1.272, *P*=0.9985, t=0.3495; layer VI, control 36.09±1.318, *Zbtb20NexKO* 38.43±2.098, *P*=0.0635, t=2.640; d.f.=30; *n*=4 mice per group; two-way ANOVA). Neuronal density in the S1 of *Zbtb20NexKO* mice was not affected (Fig. S5, individual values and mean; NEUN^{+} cells/mm^2; mean±s.d.: control 3954±387, *Zbtb20NexKO* 4239±45.42; *P*=0.1928, t=1.467, d.f.=6; *n*=4 mice per group; unpaired *t*-test; Table S3). Neuronal migration and distribution of BRN2^{+}, CTIP2^{+} and TLE4^{+} neurons were not

affected in *Zbtb20NexKO* mice (Fig. 6E, mean±s.e.m., Table S3), but the distribution of RORβ⁺ cells was shifted towards the most superficial positions of the cortex (percentage RORβ⁺cells/total; two-way ANOVA; $P<0.0001$; $n=4$ per group; Table S3). Similarly, the distribution of NEUN⁺ cells per bins was significantly different in bin 8, corresponding to the shift of layer IV towards the most superficial cortical position (Fig. S5B, mean±s.e.m., percentage NEUN⁺ cells/bins, two-way ANOVA; $P<0.0001$; $n=4$ per group; Table S3).

We next evaluated axonal projections of layer II/III CPNs in *Zbtb20NexKO* mice through pCAG-RFP expression by *in utero* electroporation at E15.5 and analysis at P14 (Fig. 7A). Electroporated cells were mainly located in layers II/III in control and *Zbtb20NexKO* mice. The number of electroporated RFP⁺ neurons was similar between the groups (Fig. 7C, individual values and mean; number of RFP⁺ neurons/mm², mean±s.d.: control 282.0±30.62, *Zbtb20NexKO* 306.5±33.16; $P=0.2136$, t=1.328, d.f.=10; $n=6$; unpaired *t*-test). RFP⁺ upper layer neurons projecting axons towards the midline were present in controls and *Zbtb20NexKO* mice with no significant difference in RFP fluorescence intensity of the CC (Fig. 7B,D, individual values and mean; RFP fluorescence in a.u.; mean±s.d.: control 54.84±7.952, *Zbtb20NEXcKO* 51.95±6.347; $P=0.5025$, t=0.6956, d.f.=10; $n=6$; unpaired *t*-test). However, a prominent reduction in the amount of axonal fibers was observed in the homotopic contralateral cortex in *Zbtb20NexKO* mice compared with controls (Fig. 7E, fluorescence intensity for RFP from the white matter to the pial surface;

mean±s.d.: control 9.05±1.749, *Zbtb20NexKO* 6.53±0.68; $n=4$ mice per group; Kolmogorov–Smirnov test; $P=0.0493$). These alterations are similar to those observed in *Zbtb20cKO* mice, although to a lesser extent.

Zbtb20 affects astrocyte development
To investigate the effects of *Zbtb20* deletion on astrocyte development, we assessed the number of astrocytes in adult *Zbtb20cKO* mice. We first stained histological sections at P42 with antibodies to S100β, GFAP and SOX9 (Fig. 8A-C). S100β is expressed by ependyma and glial lineages, mainly astroglial cells of the perinatal neocortex (Deloulme et al., 2004; Raponi et al., 2007). SOX9 is an astrocyte-specific marker in all major areas of the CNS outside of the neurogenic regions and labels the pool of astroglial cells more completely compared with S100β (Sun et al., 2017). The total number of S100β⁺ cells in S1 of *Zbtb20cKO* mice was not affected (S100β⁺ cells/mm²; mean±s.d.: control 868.0±83.54, *Zbtb20cKO* 945.7±34.56; P-value=0.2110, t=1.488, d.f.=4; $n=3$; unpaired *t*-test), but the number of SOX9⁺ cells was increased (SOX9⁺ cells/mm²; mean±s.d.: control 662.7±34.82, *Zbtb20cKO* 809.0±14.73; $P=0.0026$, t=6.704, d.f.=4; $n=3$; unpaired *t*-test).

Next, we stained sections of adult animals with antibodies to GFAP, which unlike SOX9 is expressed only in a subpopulation of mature astrocytes (Bayraktar et al., 2020). GFAP expression was confined to the pial surface and white matter in control neocortex, whereas in *Zbtb20cKO* mice GFAP expression was upregulated throughout S1 (GFAP⁺ cells/mm²; mean±s.d.: control 409.7±19.40,
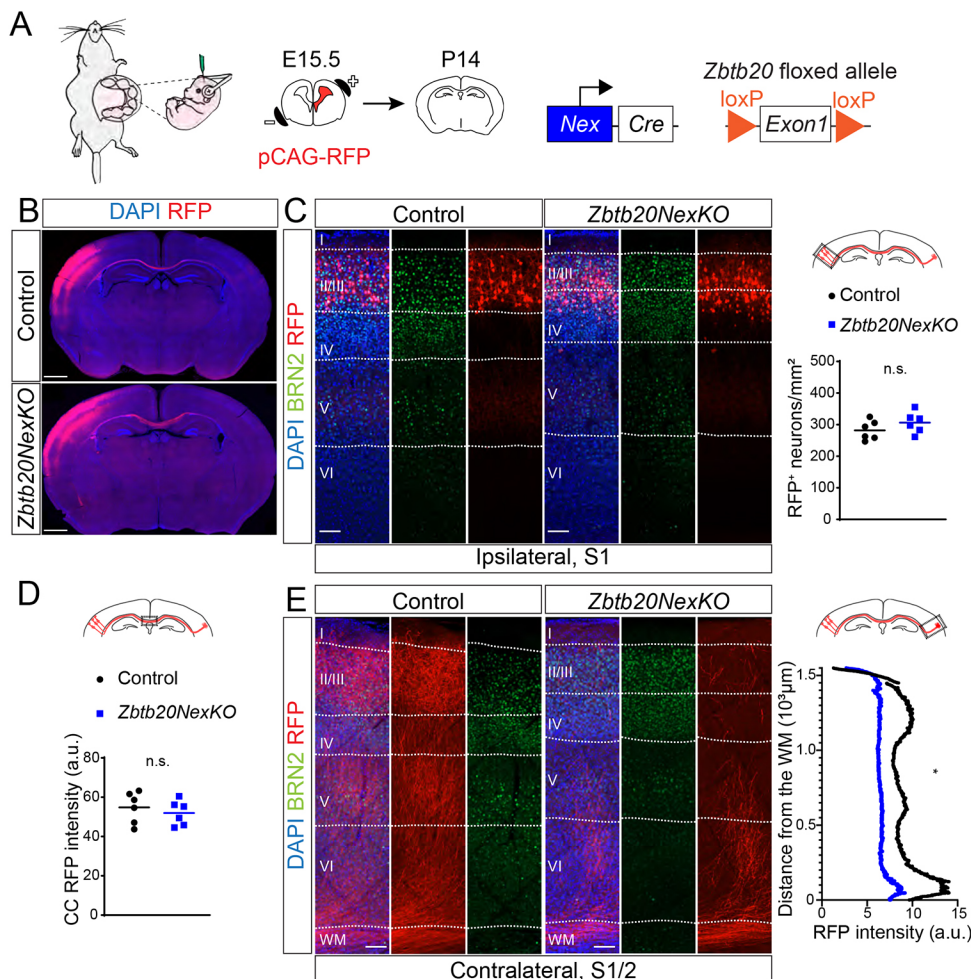

Fig. 7. Callosal projections of layer II/III neurons are affected in *Zbtb20NexKO* mice. (A) Schematic of the experimental strategy. *In utero* electroporation carried out with pCAG-RFP at E15.5, histological analysis at P14. (B) Coronal sections stained with DAPI after electroporation with pCAG-RFP. (C) Coronal sections of the electroporated (ipsilateral) hemisphere of the S1 stained with DAPI and an antibody to BRN2. RFP⁺ neurons/mm² represented as individual values and mean; $n=6$ mice/group; unpaired *t*-test. (D) Fluorescence intensity of RFP in the middle line of the CC; a.u. represented as individual values and mean; $n=6$ mice/group; unpaired *t*-test. (E) Coronal sections of the non-electroporated (contralateral) hemisphere of S1/2 stained with DAPI and an antibody to BRN2. RFP fluorescence intensity plotted from the white matter (WM) to the pial surface; $n=4$ mice/group; Kolmogorov–Smirnov test; *$P=0.0493$. n.s., not significant ($P≥0.05$). Scale bars: 100 µm (C,E); 1000 µm (B).
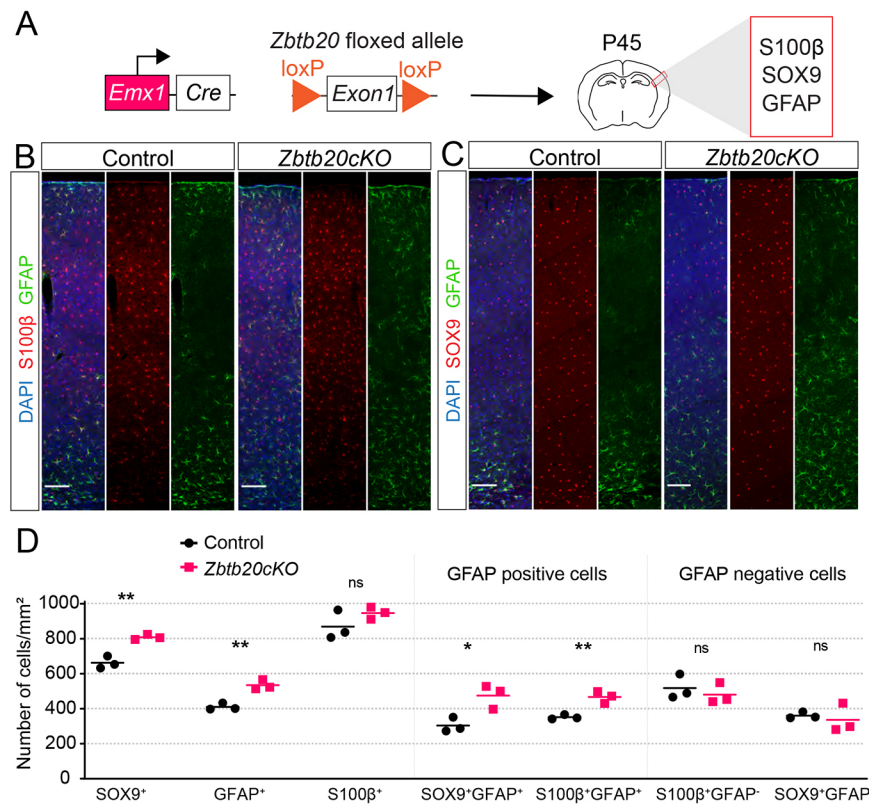
Fig. 8. Genetic inactivation of *Zbtb20* in neocortical progenitors leads to defects in astrogliogenesis. (A) Schematic of the experimental strategy. *Zbtb20flox* mice were crossed with *Emx1-Cre* mice to inactivate *Zbtb20* in progenitor cells; histological analysis for glial markers was performed at P45. (B,C) Coronal sections of the S1 stained with DAPI and antibodies to S100β and GFAP (B), or SOX9 and GFAP (C). (D) Cells/mm^2 plotted for each of the markers alone and for double labeling with GFAP. Data represented as individual values and mean; *n*=3 mice/group; unpaired *t*-test; ns, not significant (*P*≥0.05); *P<0.05; **P<0.01. Scale bars: 100 µm.

Zbtb20cKO 533.3±27.79; *P*=0.0032, t=6.320, d.f.=4; *n*=3; unpaired *t*-test) (Fig. 8B-D). Co-labeling with GFAP and SOX9 or S100β revealed an increase in the number of SOX9$^+$GFAP$^+$ and S100β$^+$GFAP$^+$ cells (SOX9$^+$GFAP$^+$ cells/mm^2; mean±s.d.: control 302.7±41.59, *Zbtb20cKO* 473.7±68.60, *P*=0.0210, t=3.692; S100β$^+$GFAP$^+$ cells/mm^2, control 350.3±13.05, *Zbtb20cKO* 465.0±33.78, *P*=0.0054, t=5.485; d.f.=4; *n*=3; unpaired *t*-test). Numbers of SOX9$^+$GFAP$^-$ and S100β$^+$GFAP$^-$ were not altered (SOX9$^+$GFAP$^-$ cells/mm^2; mean±s.d.: control 359.7±18.58, *Zbtb20cKO* 335.7±82.14, *P*=0.6474, t=0.4936, d.f.=4; S100β$^+$GFAP$^-$ cells/mm^2, control 517.7±70.51, *Zbtb20cKO* 480.7±59.53, *P*=0.5256, t=0.6944, d.f.=4; *n*=3; unpaired *t*-test). We conclude that subpopulations of astrocytes expressing GFAP are increased in *Zbtb20cKO* mice.

We next addressed whether defects in astrocyte populations already manifested during early developmental stages. We analyzed the expression of S100β, GFAP and SOX9 at P4 and P10 but found no significant difference between wild type and mutants (Fig. S6A,B) (P4: GFAP$^+$ cells/mm^2; control 256.2±48.14, *Zbtb20cKO* 237.6±28.69, *P*=0.4792, t=0.7421, d.f.=8, *n*=5, unpaired *t*-test; SOX9$^+$ cells/mm^2, control 2657±476.3, *Zbtb20cKO* 2481±755.7, *P*=0.6720, t=0.4393, d.f.=8; *n*=5, unpaired *t*-test; S100β$^+$ cells/mm^2; control 299.8±86.56, *Zbtb20cKO* 319.2±107.4, *P*=0.7612, t=0.3145, d.f.=8, *n*=5, unpaired *t*-test) (P10: GFAP$^+$ cells/mm^2; control 680.3±132.2, *Zbtb20cKO* 666.0±64.25, *P*=0.8526, t=0.1939, d.f.=6, *n*=4, unpaired *t*-test; SOX9$^+$ cells/mm^2, control 1576±153.8, *Zbtb20cKO* 1606±212.0, *P*=0.8250, t=0.2309, d.f.=6; *n*=4, unpaired *t*-test; S100β$^+$ cells/mm^2; control 1410±166.8, *Zbtb20cKO* 1276±147.3, *P*=0.2723, t=1.209, d.f.=6, *n*=4, unpaired *t*-test).

Astrocytes respond to injury by increasing expression of GFAP (Yu et al., 2009) and SOX9 (Sun et al., 2017) and increasing their rate of proliferation (Bardehle et al., 2013). To exclude the possibility that *Zbtb20cKO* mice have a reactive gliosis, we

analyzed the expression of markers for microglia (IBA1), proliferation (KI67; MKI67) and reactive astrocytes (*Serpina3n*) (Clarke et al., 2018). Immunohistochemistry revealed no differences in the number of cells expressing IBA1 or KI67 between control and *Zbtb20cKO* mice (Fig. S7A-C, IBA$^+$ cells/ mm^2; mean±s.d.; control 285.7±29.92, *Zbtb20cKO* 293.6±30.41; *P*=0.7656, t=0.3191, d.f.=4; *n*=3; unpaired *t*-test; KI67$^+$ cells/mm^2; control 44.00±1.732, *Zbtb20cKO* 43.33±7.095; *P*=0.8820, t=0.1581, d.f.=4; t=; *n*=3; unpaired *t*-test;). For *Serpina3n*, we analyzed mRNA levels by RNAScope. As a general marker for astrocytes, we analyzed in parallel mRNA expression for *Glast* (*Slc1a3*) (Bayraktar et al., 2020) (Fig. S7D). We observed no difference in the numbers of cells expressing *Serpina3n* between controls and *Zbtb20cKO* mice (Fig. S7E, *Serpina3n*$^+$*Glast*$^+$ cells/ mm^2; mean±s.d.; control 114.7±21.39, *Zbtb20cKO* 109.0±14.00; *P*=0.7205, t=0.3840, d.f.=4; *n*=3; unpaired *t*-test). However, and similar to what we observed for SOX9, the number of *Glast*$^+$ astrocytes was increased in the *Zbtb20cKO* mice (*Glast*$^+$ cells/mm^2; mean±s.d.; control 584.0±33.96, *Zbtb20cKO* 719.0±40.84; *P*=0.0117, t=4.402, d.f.=4; *n*=3; unpaired *t*-test).

These results suggest that the increase in astrocyte number in the *Zbtb20cKO* mutants most likely reflects an increase in the subtype of astrocytes expressing GFAP, which manifests after P10 without obvious signs of reactive gliosis.

A *Zbtb20* mutation causing Primrose syndrome affects astrogliogenesis

It has previously been shown that ZBTB20 overexpression and knockdown by *in utero* electroporation promotes and suppresses astrogliogenesis, respectively (Nagao et al., 2016). We were therefore surprised that we did not observe reduced numbers of astrocytes in *Zbtb20cKO* mice. We wondered whether ZBTB20 might have redundant functions with any of the other 45 known

ZBTB family members (Siggs and Beutler, 2012) during astrocyte development. Overexpression of ZBTB20 alone might facilitate astrocyte development and knockdown might have affected other ZBTB family members as well.

To identify other ZBTB gene family members expressed in the developing neocortex, we carried out quantitative RT-PCR experiments with RNA isolated from the dorsal telencephalon of E18.5 control and *Zbtb20cKO* embryos at the time of onset of astrogliogenesis. mRNA levels of *Zbtb4*, *Zbtb6*, *Zbtb7c*, *Zbtb11*, *Zbtb20*, *Zbtb27* (*Bcl6*) and *Zbtb45* were mildly downregulated in

Zbtb20cKO mice compared with controls, whereas the expression of *Zbtb2*, *Zbtb3*, *Zbtb18*, *Zbtb31* (*Mynn*), *Zbtb40* and *Zbtb48* were mildly upregulated (Fig. 9A, Table S3). Other ZBTB family members were unaffected (Fig. S8, Table S3).

Because a large number of ZBTB family members are expressed in the developing neocortex, it was not practical to investigate all of them through the generation of genetically modified mice. We therefore took advantage of the observation that Primrose syndrome is associated with dominant-negative *ZBTB20* mutations (Cordeddu et al., 2014). Given the widespread pathological changes associated
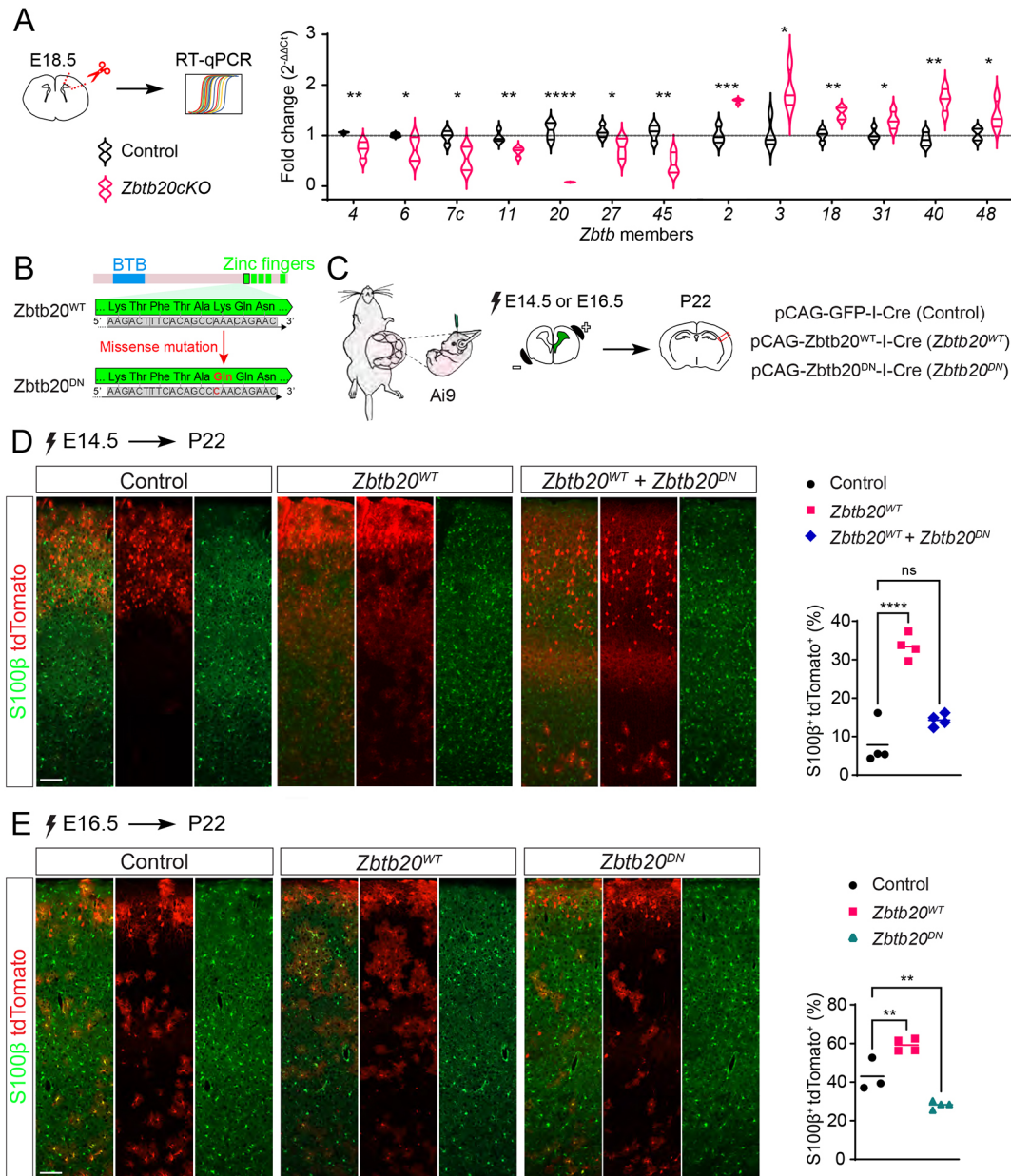

Fig. 9. Overexpression of a dominant-negative ZBTB20 protein in cortical progenitors affects astrogliogenesis. (A) Schematic showing dissection of the dorsal telencephalon at E18.5 in control and *Zbtb20cKO* embryos, followed by RNA extraction, and RT-qPCR for genes encoding ZBTB family members. Violin plots represent fold change expression of each ZBTB family member relative to the controls ($2^{-\Delta\Delta Ct}$). ZBTB gene numbers are listed on the *x*-axis. *Gapdh* was used as an endogenous control for all samples. Data represented as quartiles and median values; *n*=4 mice/group; unpaired *t*-test. (B) Schematic showing ZBTB20 protein domains and the dominant-negative mutation (A>C, Lys590Gly) in the zinc-finger domain. (C) Schematic of the experimental strategy. *In utero* electroporation was carried out in Ai9 mice at E14.5 or E16.5 with the indicated plasmids. Histological analysis was performed at P22. (D,E) Coronal sections of S1 at P22 stained for DAPI, tdTomato and with an antibody to S100β. Electroporation with the indicated plasmids were carried out at E14.5 (D) and E16.5 (E). DN, dominant negative; I, IRES; p, promoter; WT, wild type. Data are represented as individual values and mean; *n*=4 mice/group; unpaired *t*-test; ns, not significant ($P \geq 0.05$); **$P < 0.01$; ****$P < 0.0001$. Scale bars: 100 μm.

with Primrose syndrome, and that ZBTB20 participates in homo- and heterotypic protein interactions (Mitchelmore et al., 2002), dominant-negative mutations could affect the function of other ZBTB family members. We therefore expressed by *in utero* electroporation wild-type *Zbtb20* (*Zbtb20^{wt}*) or *Zbtb20* carrying a Primrose mutation (A>C and Lys590Gln; referred as *Zbtb20^{DN}*) in the neocortex of mice (Fig. 9B-E).

To identify cells that had taken up the DNA and their offspring, experiments were carried out with Ai9 mice and plasmids that also expressed Cre to activate td-Tomato expression in the electroporated cells. A plasmid expressing only Cre served as a control (Fig. 9C). *Zbtb20^{WT}* was expressed at E14.5, prior to the onset of astrogliogenesis. As reported earlier (Nagao et al., 2016), at P22 we observed a significant increase in the number of S100β$^+$ astrocytes in the neocortex of mice electroporated to express *Zbtb20^{WT}* (Fig. 9D). This increase was suppressed by concomitant expression of *Zbtb20^{DN}* with *Zbtb20^{WT}* [percentage S100β$^+$ and tdTomato$^+$/total tdTomato$^+$ cells; mean±s.d.; control 7.857±5.574, *Zbtb20^{WT}* 33.39±3.190, *Zbtb20^{WT}*+*Zbtb20^{DN}* 14.28±1.661; $P<0.0001$, $F(2, 9)=48.10$; $n=4$; ANOVA] (Fig. 9D). Next, we expressed *Zbtb20^{DN}* at E16.5 when *Zbtb20* expression is prominent within cortical progenitors. Notably, expression of *Zbtb20^{WT}* led to a significant increase in the number of S100β$^+$ astrocytes, whereas *Zbtb20^{DN}* significantly reduced the number of S100β$^+$ astrocytes [Fig. 9E; percentage S100β$^+$tdTomato$^+$ cells; mean±s.d.: control 43.03±8.392, *Zbtb20^{WT}* 59.18±3.302, *Zbtb20^{DN}* 28.26±2.003, $P<0.0001$, $F(2, 8)=41.24$; $n=3$ control and $n=4$ *Zbtb20^{WT}* and *Zbtb20^{DN}*; ANOVA]. We thus conclude that ZBTB20 might cooperate with other ZBTB family members to regulate astrogliogenesis.

DISCUSSION

We provide here evidence that the transcription factor ZBTB20 is a crucial regulator of cell-type specification in the developing neocortex affecting both glutamatergic neurons and astrocytes. First, our findings demonstrate that ZBTB20 is essential for the specification of a subset of CPNs in layer II/III. When the expression of ZBTB20 is disrupted in the developing neocortex, an increase in the number of layer IV neurons is observed at the expense of layer II/III neurons. Conversely, ZBTB20 overexpression in neocortical progenitors switches neuronal fates from layer IV to layers II/III. Consistent with the onset of expression of ZBTB20 around the time when layer II/III neurons are born (E15.5), specification of the earlier born layer V and VI neurons is not affected by loss of ZBTB20. Second, we demonstrate that astrocyte numbers are increased in adult *ZBTB20cKO* mice with an increase in the subtype expressing GFAP. A dominant-negative ZBTB20 construct associated with Primrose syndrome affects astrogliogenesis more severely than a knockout of *Zbtb20* alone, suggesting that ZBTB20 acts together with other transcriptional regulators that were affected by the dominant-negative construct to instruct astrogliogenesis. Taken together, our findings provide new insights into the function of ZBTB20 in the neocortex and suggest that defects in cell-type specification contribute to the pathological changes associated with dominant *ZBTB20* mutations found in individuals with Primrose syndrome.

Previous investigations that were based on the study of mice with null mutations in *Zbtb20* had suggested that ZBTB20 is essential for the sequential generation of neuronal layers in developing neocortex (Tonchev et al., 2016). However, *Zbtb20*-null mice die after birth when cortical development is still in progress (Rosenthal et al., 2012). We therefore analyzed mice in which *Zbtb20* was conditionally inactivated specifically in the developing neocortex,

thus preventing the lethality associated with *Zbtb20*-null alleles. We show that loss of *Zbtb20* does not affect the formation of layer V and VI neurons, which is consistent with the fact that ZBTB20 is not expressed in cortical progenitor cells when these neurons are generated. Previous studies used *Zbtb20*-null mice that lack ZBTB20 in all tissues (Tonchev et al., 2016). Perhaps the reported effects in layer V and VI neurons were caused indirectly by defects in other tissues. Instead, we show here that in *Zbtb20cKO* mice the development of a subset of CPNs in layer II/III is affected. These defects were most prominent when *Zbtb20* was inactivated with *Emx1-Cre* in progenitors, but to a lesser extent also following inactivation with *Nex-Cre* in postmitotic neurons. This suggests that *Zbtb20* acts both in progenitors and differentiating neurons to instruct the generation of neurons expressing layer II/III markers. This finding is consistent with the observation that *Zbtb20* is expressed in progenitor cells and transiently in a subset of BRN2$^+$ layer II/III neurons (Tonchev et al., 2016). In addition, our *in utero* electroporation experiments show that overexpression of ZBTB20 at E14.5 is sufficient to induce the premature differentiation of layer II/III neurons at the expense of layer IV neurons. Notably, the reduction in the number of neurons expressing markers for layer II/III was far greater than the changes in the size of the CC, suggesting that some neurons might be only partially re-specified from a callosal phenotype. ZBTB20 thus joins a group of transcriptional regulators including FEZF2, CTIP2, TBR1, SOX5, SATB2, BRN1 (POU3F3) and BRN2 (POU3F2) that have instructive roles in the generation of subtypes of cortical projection neurons (Greig et al., 2013; Molyneaux et al., 2007).

We show here that the loss of ZBTB20 in progenitors and immature neurons also affects two important aspects of neuronal circuit formation: (1) organization of thalamocortical projections; and (2) inter-hemispheric connections. Accordingly, the increased radial distribution of RORβ$^+$ neurons was accompanied by an increase in the arborization of thalamocortical fibers, leading to an expansion of barrel areas in S1. Furthermore, we observed a severe reduction in callosal projections of upper layer neurons in the contralateral hemisphere of *Zbtb20cKO* mice, which is consistent with the reduction in the number of layer II/III neurons. Interestingly, axons of remaining CPNs in the mutant mice are able to cross the midline and reach the contralateral homotopic white matter but fail to invade the cortical plate, reach superficial layers, and ramify as control CPNs. This defect could indicate cell-autonomous defects in the remaining CPNs that projected across the midline but could also be a consequence of non-autonomous defects caused by perturbations of the neuronal layers invaded by the axons. Notably, deep layer CPNs, which are unaffected by *Zbtb20* deletion, properly innervate the contralateral layer V.

Our findings also shed light on the role of *Zbtb20* in astrogliogenesis. Based on *in utero* electroporation experiments, it had been proposed that *Zbtb20* instructs astrogliogenesis (Nagao et al., 2016). We were able to replicate these *in utero* electroporation results. However, our genetic experiments demonstrate that astrogliogenesis can occur in the absence of expression of endogenous *Zbtb20*. Astrocyte numbers were even increased in adult animals with an expansion of the subtype of astrocytes expressing GFAP. The observation that ZBTB20 is expressed in progenitor cells during astrogliogenesis, and that overexpression of ZBTB20 can induce the formation of an increased number of astrocytes, suggests that it might have a permissive function in astrogliogenesis. Notably, ZBTB20 is a member of a large family of transcriptional regulators with extensive sequence homology especially in the DNA-binding domain (Siggs and Beutler, 2012).

We show that several ZBTB20 family members are expressed in the developing neocortex at the onset of astrogliogenesis. Furthermore, a dominant-negative ZBTB20 protein associated with Primrose syndrome affects the generation of astrocytes. Although further studies are necessary, these findings are consistent with a model in which two or more ZBTB family members have redundant functions in astrogliogenesis.

In summary, our findings shed new light on the function of Zbtb20 and suggest that it has crucial roles for the generation of appropriate numbers of specific subtypes of neurons and astrocytes. Defects in cell-type specification are therefore likely to be a factor in the molecular pathogenesis of Primrose syndrome.

MATERIALS AND METHODS
Mouse lines and breeding
All animal experiments were approved by the Institutional Animal Care and Use Committee at Johns Hopkins University School of Medicine. Mice were maintained on a 14 h light/10 h dark cycle. Both male and female mice were used, and no obvious differences between the sexes were noted. All mice were group-housed in pathogen-free facilities with regulated temperature and humidity and given *ad libitum* access to food and water. All of the mice used were seemingly free of infection, health abnormalities or immune system deficiencies. None of the mice used had been used for previous experiments.

C57BL/6J wild-type (WT) mice were obtained from Charles River Laboratories. The date of the vaginal plug detection was designated E0.5, and the date of birth P0.

Emx1-Cre [B6.129S2-*Emx1tm1(cre)Krj*] (Gorski et al., 2002), *Ai9* (Madisen et al., 2010), *Nex-Cre* (Goebbels et al., 2006) and *FLPe* [B6.Cg-Tg(ACTFLPe)9205Dym/J] (Rodríguez et al., 2000) mice have been described.

Zbtb20 knockout-first allele with conditional potential embryonic stem cells (ESCs) [*Zbtb20tm1a*(EUCOMM)Hmgu] were obtained from the EUCOMM European Conditional Mouse Mutagenesis Program (ES clone HEPD0822_1_A11). The ESCs were designed to insert LoxP sites flanking a critical exon of the *Zbtb20* gene, with upstream elements including a neomycin-resistance cassette (PGK-neo) and *lacZ* reporter flanked by two FRT sites. ESCs were transplanted into mouse blastocysts by The Scripps Research Murine Genetics Core (La Jolla, CA, USA) to produce transgenic mice. Heterozygous F1 mice (*Zbtb20flox-neo/+*) were mated with *FLPe* mice to remove the PGK-neo cassette and *lacZ* reporter. The resulting offspring were subsequently mated to C57BL/6J mice to remove the FLPe transgene.

Plasmid constructs
Dominant-negative mutations of *Zbtb20* and Cre recombinase were expressed under the control of the CAG promoter (pCAG-Zbtb20^{wt}-IRES-Cre). The coding sequence for *Zbtb20* was amplified from mouse cDNA by PCR. Isoform 1 of *Zbtb20* including the first nine nucleotides before the ATG (Kozak sequence) was amplified. Restriction enzyme sites were added to the primer sequence, and fragments were cloned into the pCAG-IRES-Cre construct. Human dominant-negative mutations of *ZBTB20* were introduced into the mouse cDNA by PCR amplification using mega primers. All constructs were sequenced to confirm the point mutation. We cloned a *ZBTB20* mutation described in individuals with Primrose syndrome by Cordeddu and colleagues (2014); this mutation is located in the first C terminus zinc-finger domain (#1768). The number of the mutation used here refers to the altered nucleotide position in the longer transcript variant sequence (NCBI Reference Sequence: NM_001164342.1), which corresponds to the following nucleotide and amino acid changes, respectively: 1768A>C and Lys590Gln. This mutation affects the DNA-binding domain of the transcription factor possibly through dominant-negative action (Cordeddu et al., 2014). This mutation exhibited the strongest effect with respect to reduced binding to DNA, led to impaired function in repressing luciferase reporter expression under the control of the promoter for AFP (encoding α-fetoprotein), known to contain a ZBTB20 recognition site, and had a dominant-negative impact on wild-type ZBTB20 (Cordeddu et al., 2014).

In utero electroporation
The protocol described here was adapted from Saito and Nakatsuji (2001). Timed pregnant mice were placed in an induction chamber and anesthetized with 3% isoflurane in 21% oxygen. Eye lubricant (Puralube Vet Ointment) was applied to prevent damage and mice were then transferred to a heated blanket connected to the anesthesia machine with a nose mask. During the surgical procedure, mice were anesthetized with 2% isoflurane in 21% oxygen and 5 mg/kg carprofen in saline (OstiFen Injection Sterile Injectable Solution, 50 mg/ml, VetOne) was injected subcutaneously for pain relief. Respiratory rate was closely observed and the mouse's response to a noxious stimulus (toe pinch) was verified to ensure adequate anesthesia before proceeding.

Plasmid DNA (2 µg/µl) with 1/20 volume of 1% Fast Green (#F7252, Sigma-Aldrich) in TE buffer was injected into the embryos' lateral ventricles through a beveled glass micropipette. Sterile saline solution (37°C) was constantly applied to moisturize the embryos. The embryo's head was held using tweezers with disk electrodes (3 or 5 mm diameter electrode disk; CUY650P3 and CUY650P5, respectively, Sonidel Limited) with the positive electrode contacting the dorsolateral region of the injected side (for selective targeting the somatosensory cortex). Five electric pulses of 30-50 V and 50-80 ms were delivered at a rate of one pulse per 950 ms using an electroporation system (ECM 830 BTX, Harvard Apparatus) with a foot-controlled pedal.

Upon completion of the injection and electroporation of all desired embryos, the uterine horns were carefully inserted back into the abdominal cavity filled with saline solution (37°C). The surgical incision was closed with absorbable suture, then the skin was sutured (with suture or wound clips). Triple antibiotic ointment (containing Polymyxin B, Bacitracin and Neomycin) was applied to prevent infection. The females were kept warm to recover from anesthesia, and they were closely monitored for the first few hours post-surgery.

Immunohistochemistry
Embryonic brains were fixed in 4% paraformaldehyde (PFA; #15710, and #15714, Electron Microscopy Sciences) in PBS (#MB1001, BioPioneer) for 4-8 h at 4°C. Postnatal mice were transcardially perfused with 20-25 ml ice-cold 4% PFA using a peristaltic pump at a rate of 2-2.5 ml/min. Brains were removed from the skull and postfixed in 4% PFA overnight at 4°C shaker. Brains were washed with PBS three times for 10 min each, embedded in 4% low melting point agarose (#AGAL0050, MP Biomedicals; #R0801, Thermo Fisher Scientific) in PBS, and were sectioned coronally at 100 µm or 50 µm with a vibrating microtome (VT1200S, Leica).

Free floating sections were incubated for 1 h in blocking solution (10% normal goat serum or fetal bovine serum and 0.1% Triton X-100 in PBS). The primary antibodies, diluted in blocking solution, were applied, and the sections were incubated overnight (or 48 h depending on the thickness of the section and antibody used) at 4°C on a shaker. The sections were then rinsed three times for 10 min each in PBS and subsequently incubated with the appropriate secondary antibodies diluted in blocking solution for 2 h at room temperature. To label all cell nuclei, the fluorescent nuclear dye DAPI (1 µg/ml, Sigma-Aldrich) was included with the secondary antibody solution. After a final set of rinses, three times for 10 min each with PBS, the sections were mounted on slides with mounting medium (ProLong Gold, Thermo Fisher Scientific). All the antibodies and respective concentrations used are listed in Table S1.

Antigen retrieval was required to stain for RORβ, and the method greatly improved other nuclear stains, such as NEUN, CTIP2, ZBTB20, TLE4 and BRN2. The protocol used here was a heat-induced citrate method (Tang et al., 2007). Free-floating sections were washed in PBS for 15 min and the sections were steamed in citrate buffer (10 mM sodium citrate, 0.05% Tween20, pH 6.0) for 15 min at 97-98°C (Black and Decker Handy Steamer). A digital thermometer (Thermo Fisher Scientific) was placed on the rack to allow continuous monitoring of the temperature. After steaming, the sections were allowed to cool at room temperature for 2-5 min. Once again, they were washed in PBS for 15 min at room temperature and the conventional immunohistochemistry protocol described above was followed.

RNAScope multiplex *in situ* hybridization

Postnatal mice were transcardially perfused with 4% PFA and brains were postfixed overnight in 4% PFA at 4°C. Brains were washed with PBS three times, cryoprotected with 30% sucrose, and embedded with embedding compound (Tissue-Tek O.C.T.) for cryosectioning. Sixteen-μm coronal sections were then processed for multiplex fluorescent *in situ* hybridization RNAScope (Wang et al., 2012) following the manufacturer's instructions (RNAScope Multiplex Fluorescent V2, Advanced Cell Diagnostics). Briefly, sections were treated with hydrogen peroxide, target retrieval solution, protease, and hybridized with gene-specific probes to mouse *Glast* (430781-C2) and *Serpina3n* (430191).

Retrograde labeling

Anesthetized mice were place under the microscope at P30 and ∼0.5 μl of Red Retrobeads IX (#R180, Lumafluor) was injected into S1. The mice were transcardially perfused at P36 and brains were processed using the same protocol described above for immunohistochemistry.

RNA extraction and RT-qPCR

E18.5 embryos were dissected in cold Hanks' Balanced Salt Solution (HBSS; 14175-095, Gibco) with HEPES (15630080, Gibco). Embryos were kept on ice while dorsal telencephalon dissection was performed (Landeira et al., 2017). Tissue was collected in Eppendorf tubes on ice. RNA extraction was performed following the manufacturer's instructions (Aurum Total RNA Mini Kit, 732-6820, Bio-Rad; QIAshredder, 79654, Qiagen). RNA concentration was measured using the spectrophotometer. The samples were aliquoted and stored at −80°C.

RNA samples were reverse transcribed into DNA using a high-fidelity cDNA synthesis kit (iScript Select cDNA Synthesis Kit, 170-8897 or iScript cDNA Synthesis Kit, 1708890; both from Bio-Rad). The samples were diluted in endonuclease-free water (4 ng/μl). Real-time quantitative PCR (RT-qPCR) reactions were prepared using a 2× SYBR Green mix (SSoAdvanced universal SYBR Green Supermix, Bio-Rad), 5 μM reverse primer, 5 μM forward primer and 625 nM cDNA and 20 μl of the reaction mixture per well was placed in a 96-well plate (MicroAmp Optical 96-Well Reaction Plate, N8010560, Thermo Fisher Scientific). The RT-qPCR reactions were run on the QuantStudio 6 Flex Real-Time PCR System (Applied Biosystems).

RT-qPCR primers and analysis

Primers were designed using online tools: Integrated DNA Technologies' RealTime qPCR tool (//idtdna.com/scitools/Applications/RealTimePCR/) and Universal ProbeLibrary Assay Design Center (//lifescience.roche.com/en_us/brands/universal-probe-library.html#assay-design-center). Primer-BLAST was used to check target specificity (//ncbi.nlm.nih.gov/tools/primer-blast/) and NetPrimer was used to analyze primers' characteristics, such as melting temperature, secondary structure, and complementarity of each pair of primers (//premierbiosoft.com/NetPrimer/AnalyzePrimer.jsp). Nucleotide sequences of primers used are listed in Table S2.

In this experiment, the dorsal telencephalon of four controls and four conditional knockout E18.5 embryos were used to verify the expression of ZBTB family members. Each sample was run in duplicates. The cycle threshold value or Ct was used to calculate the relative fold gene expression of the samples. ΔCt was calculated for each sample by subtracting the average *Gapdh* Ct from the Ct of each gene of interest. ΔΔCt was calculated by subtracting the ΔCt of each ZBTB family member from the average ΔCt of the control group (the reference sample). Fold change expression ($2^{-\Delta\Delta Ct}$) of each ZBTB family member in relation to the control group expression is represented as violin plots (linear scale).

Image analysis and quantification

Images were captured using a Keyence Microscope, a Zeiss Axio Zoom microscope, a Zeiss Cell Observer microscope system, a Nikon-A1 laser-scanning confocal, a Zeiss LSM 800 confocal and a Zeiss LSM 700 confocal. Image analysis and cell quantification were performed using ZEN, Imaris and ImageJ. All immunohistochemistry data were acquired in at least three distinct rostrocaudal coronal sections of each brain. A series of *z*-stack (depth of 10 μm at *z*-plane) confocal tiled images were used for cell

quantification; 350-μm-wide images comprising the entire extension of cortical plate (∼1000-1400 μm long) were analyzed. In all fluorescence microscopy figures, different channels of image series were combined in pseudocolor, and contrast and brightness were adjusted manually using ZEN or Adobe Photoshop CS6. Maximum intensity projections were generated in ImageJ, ZEN or Imaris.

The total number of cells was quantified in a radial section of the primary somatosensory cortex (S1) and adjusted per area. To divide the cortical plate into longitudinal bins, a rectangle was drawn from the border of the white matter with layer VI to the pial surface. This rectangle was then divided into ten equal bins and the number of cells within each bin was quantified.

The contribution of individual layers to the cortical thickness was visually distinguished by the expression of cortical projection neuron markers. The radial fraction occupied by neurons expressing BRN2 only was considered layer II/III; high levels of RORβ, layer IV; high levels of CTIP2, layer V; both TLE4 and CTIP2, layer VI; not labeled for any of those markers, layer I. All neuronal makers were counterstained with DAPI to allow visualization of overall cellular density and proper distinction of each layer.

Axonal ramification of callosal neurons in the contralateral hemisphere was indirectly measured as fluorescence intensity using ImageJ. A rectangular box comprising the white matter and cortical layers I to VI was drawn and the profile of fluorescence distribution from the white matter to the pial surface was plotted in a.u.

RFP fluorescence intensity of the CC was measured using ImageJ. A rectangular box including the CC at the midline was drawn and the average fluorescence intensity for each mouse was plotted in a.u.

Experimental design and statistical analysis

Mean, s.d. and s.e.m. were calculated and statistical analyses were performed using GraphPad Prism. Statistically significant differences of means were assessed by Student's unpaired *t*-test or two-way analysis of variance (ANOVA), comparing two or more groups, respectively. $P < 0.05$ was considered a significant difference. Frequency distributions were compared using Kolmogorov–Smirnov test. The confidence interval (CI) used in this work is 95% (*$P < 0.05$; **$P < 0.01$; ***$P < 0.001$; ****$P < 0.0001$). The exact P-values, mean±s.d., t value, degrees of freedom (d.f.), *n* and statistical test applied are reported in the Results section and in Table S3 (RT-qPCR data and cellular distribution among bins and layers). Graphs represent individual values and mean (of the number of positive cells/mm^2 or of the percentage of cells in each layer), mean±s.e.m. (percentage of positive cells in each bin/total number), and quartiles and median values (violin plots).

14

Peer review history

The peer review history is available online at https://journals.biologists.com/dev/article-lookup/doi/10.1242/dev.196642

References

Alby, C., Boutaud, L., Bessières, B., Serre, V., Rio, M., Cormier-Daire, V., de Oliveira, J., Ichkou, A., Mouthon, L., Gordon, C. T. et al. (2018). Novel de novo ZBTB20 mutations in three cases with Primrose syndrome and constant corpus callosum anomalies. *Am. J. Med. Genet. Part A* **176**, 1091-1098. doi:10.1002/ajmg.a.38684

Alcamo, E. A., Chirivella, L., Dautzenberg, M., Dobreva, G., Fariñas, I., Grosschedl, R. and McConnell, S. K. (2008). Satb2 regulates callosal projection neuron identity in the developing cerebral cortex. *Neuron* **57**, 364-377. doi:10.1016/j.neuron.2007.12.012

Arlotta, P., Molyneaux, B. J., Jabaudon, D., Yoshida, Y. and Macklis, J. D. (2008). Ctip2 controls the differentiation of medium spiny neurons and the establishment of the cellular architecture of the striatum. *J. Neurosci.* **28**, 622-632. doi:10.1523/JNEUROSCI.2986-07.2008

Bandeira, F., Lent, R. and Herculano-Houzel, S. (2009). Changing numbers of neuronal and non-neuronal cells underlie postnatal brain growth in the rat. *Proc. Natl. Acad. Sci. USA* **106**, 14108-14113. doi:10.1073/pnas.0804650106

Bardehle, S., Krüger, M., Buggenthin, F., Schwausch, J., Ninkovic, J., Clevers, H., Snippert, H. J., Theis, F. J., Meyer-Luehmann, M., Bechmann, I. et al. (2013). Live imaging of astrocyte responses to acute injury reveals selective juxtavascular proliferation. *Nat. Neurosci.* **16**, 580-586. doi:10.1038/nn.3371

Bayraktar, O. A., Bartels, T., Holmqvist, S., Kleshchevnikov, V., Martirosyan, A., Polioudakis, D., Ben Haim, L., Young, A. M. H., Batiuk, M. Y., Prakash, K. et al. (2020). Astrocyte layers in the mammalian cerebral cortex revealed by a single-cell in situ transcriptomic map. *Nat. Neurosci.* **23**, 500-509. doi:10.1038/s41593-020-0602-1

Belvindrah, R., Graus-Porta, D., Goebbels, S., Nave, K.-A. and Müller, U. (2007). B1 integrins in radial glia but not in migrating neurons are essential for the formation of cell layers in the cerebral cortex. *J. Neurosci.* **27**, 13854-13865. doi:10.1523/JNEUROSCI.4494-07.2007

Casertano, A., Fontana, P., Hennekam, R. C., Tartaglia, M., Genesio, R., Dieber, T. B., Ortega, L., Nitsch, L. and Melis, D. (2017). Alterations in metabolic patterns have a key role in diagnosis and progression of primrose syndrome. *Am. J. Med. Genet. Part A* **173**, 1896-1902. doi:10.1002/ajmg.a.38124

Catapano, L. A., Arnold, M. W., Perez, F. A. and Macklis, J. D. (2001). Specific neurotrophic factors support the survival of cortical projection neurons at distinct stages of development. *J. Neurosci.* **21**, 8863-8872. doi:10.1523/JNEUROSCI.21-22-08863.2001

Clarke, L. E., Liddelow, S. A., Chakraborty, C., Münch, A. E., Heiman, M. and Barres, B. A. (2018). Normal aging induces A1-like astrocyte reactivity. *Proc. Natl. Acad. Sci. USA* **115**, E1896-E1905. doi:10.1073/pnas.1800165115

Cleaver, R., Berg, J., Craft, E., Foster, A., Gibbons, R. J., Hobson, E., Lachlan, K., Naik, S., Sampson, J. R., Sharif, S. et al. (2019). Refining the Primrose syndrome phenotype: a study of five patients with ZBTB20 de novo variants and a review of the literature. *Am. J. Med. Genet. Part A* **179**, 344-349. doi:10.1002/ajmg.a.61024

Cordeddu, V., Redeker, B., Stellacci, E., Jongejan, A., Fragale, A., Bradley, T. E. J., Anselmi, M., Ciolfi, A., Cecchetti, S., Muto, V. et al. (2014). Mutations in ZBTB20 cause Primrose syndrome. *Nat. Genet.* **46**, 815-817. doi:10.1038/ng.3035

Davies, M. N., Krause, L., Bell, J. T., Gao, F., Ward, K. J., Wu, H., Lu, H., Liu, Y., Tsai, P.-C., Collier, D. A. et al. (2014). Hypermethylation in the ZBTB20 gene is associated with major depressive disorder. *Genome Biol.* **15**, R56. doi:10.1186/gb-2014-15-4-r56

Deloulme, J. C., Raponi, E., Gentil, B. J., Bertacchi, N., Marks, A., Labourdette, G. and Baudier, J. (2004). Nuclear expression of S100B in oligodendrocyte progenitor cells correlates with differentiation toward the oligodendroglial lineage and modulates oligodendrocytes maturation. *Mol. Cell. Neurosci.* **27**, 453-465. doi:10.1016/j.mcn.2004.07.008

Dominguez, M. H., Ayoub, A. E. and Rakic, P. (2013). POU-III transcription factors (Brn1, Brn2, and Oct6) influence neurogenesis, molecular identity, and migratory destination of upper-layer cells of the cerebral cortex. *Cereb. Cortex* **23**, 2632-2643. doi:10.1093/cercor/bhs252

Ge, W.-P., Miyawaki, A., Gage, F. H., Jan, Y. N. and Jan, L. Y. (2012). Local generation of glia is a major astrocyte source in postnatal cortex. *Nature* **484**, 376-380. doi:10.1038/nature10959

Goebbels, S., Bormuth, I., Bode, U., Hermanson, O., Schwab, M. H. and Nave, K.-A. (2006). Genetic targeting of principal neurons in neocortex and hippocampus of NEX-Cre mice. *Wiley Interscipl. Rev. Dev. Biol.* **44**, 611-621. doi:10.1002/dvg.20256

Gorski, J. A., Talley, T., Qiu, M., Puelles, L., Rubenstein, J. LR. and Jones, K. R. (2002). Cortical excitatory neurons and glia, but not GABAergic neurons, are produced in the Emx1-expressing lineage. *J. Neurosci.* **22**, 6309-6314. doi:10.1523/JNEUROSCI.22-15-06309.2002

Greig, L. C., Woodworth, M. B., Galazo, M. J., Padmanabhan, H. and Macklis, J. D. (2013). Molecular logic of neocortical projection neuron specification, development and diversity. *Nat. Rev. Neurosci.* **14**, 755-769. doi:10.1038/nrn3586

Harwell, C. C., Fuentealba, L. C., Gonzalez-Cerrillo, A., Parker, P. RL., Gertz, C. C., Mazzola, E., Garcia, M. T., Alvarez-Buylla, A., Cepko, C. L. and Kriegstein, A. R. (2015). Wide dispersion and diversity of clonally related inhibitory interneurons. *Neuron* **87**, 999-1007. doi:10.1016/j.neuron.2015.07.030

Ivy, G. O. and Killackey, H. P. (1982). Ontogenetic changes in the projections of neocortical neurons. *J. Neurosci.* **2**, 735-743. doi:10.1523/JNEUROSCI.02-06-00735.1982

Jabaudon, D., Shnider, S., Tischfield, D., Galazo, M. and MacKlis, J. D. (2012). RORβ induces barrel-like neuronal clusters in the developing neocortex. *Cereb. Cortex* **22**, 996-1006. doi:10.1093/cercor/bhr182

Jones, K. A., Luo, Y., Dukes-Rimsky, L., Srivastava, D. P., Koul-Tewari, R., Russell, T. A., Shapiro, L. P., Srivastava, A. K. and Penzes, P. (2018). Neurodevelopmental disorder-associated ZBTB20 gene variants affect dendritic and synaptic structure. *PLoS ONE* **13**, e0203760. doi:10.1371/journal.pone.0203760

Koul, R. (2014). Functional characterization of ZBTB20 and the role of ZBTB20-dependent transcription regulation in autism spectrum disorders and intellectual disability. *PhD thesis*, Clemson University, SC, USA. https://tigerprints.clemson.edu/all_dissertations/1778.

Landeira, B. S., Araújo, J. AM., Schroeder, T., Müller, U. and Costa, M. R. (2017). Live imaging of primary cerebral cortex cells using a 2D culture system. *J. Vis. Exp.* **2017**, 1-14. doi:10.3791/56063

Leone, D. P., Heavner, W. E., Ferenczi, E. A., Dobreva, G., Huguenard, J. R., Grosschedl, R. and McConnell, S. K. (2015). Satb2 regulates the differentiation of both callosal and subcerebral projection neurons in the developing cerebral cortex. *Cereb. Cortex* **25**, 3406-3419. doi:10.1093/cercor/bhu156

MacDonald, J. L., Fame, R. M., Gillis-Buck, E. M. and Macklis, J. D. (2018). Caveolin1 identifies a specific subpopulation of cerebral cortex callosal projection neurons (CPN) including dual projecting cortical callosal/frontal projection neurons (CPN/FPN). *eNeuro* **5**, 1-17. doi:10.1523/ENEURO.0234-17.2017

Madisen, L., Zwingman, T. A., Sunkin, S. M., Oh, S. W., Zariwala, H. A., Gu, H., Ng, L. L., Palmiter, R. D., Hawrylycz, M. J., Jones, A. R. et al. (2010). A robust and high-throughput Cre reporting and characterization system for the whole mouse brain. *Nat. Neurosci.* **13**, 133-140. doi:10.1038/nn.2467

Mattioli, F., Piton, A., Gérard, B., Superti-Furga, A., Mandel, J.-L. and Unger, S. (2016). Novel de novo mutations in ZBTB20 in Primrose syndrome with congenital hypothyroidism. *Am. J. Med. Genet. Part A* **170**, 1626-1629. doi:10.1002/ajmg.a.37645

Miller, F. D. and Gauthier, A. S. (2007). Timing is everything: making neurons versus glia in the developing cortex. *Neuron* **54**, 357-369. doi:10.1016/j.neuron.2007.04.019

Mitchelmore, C., Kjærulff, K. M., Pedersen, H. C., Nielsen, J. V., Rasmussen, T. E., Fisker, M. F., Finsen, B., Pedersen, K. M. and Jensen, N. A. (2002). Characterization of two novel nuclear BTB/POZ domain zinc finger isoforms. Association with differentiation of hippocampal neurons, cerebellar granule cells, and macroglia. *J. Biol. Chem.* **277**, 7598-7609. doi:10.1074/jbc.M110023200

Molyneaux, B. J., Arlotta, P., Menezes, J. RL. and Macklis, J. D. (2007). Neuronal subtype specification in the cerebral cortex. *Nat. Rev. Neurosci.* **8**, 427-437. doi:10.1038/nrn2151

Molyneaux, B. J., Goff, L. A., Brettler, A. C., Chen, H.-H., Brown, J. R., Hrvatin, S., Rinn, J. L. and Arlotta, P. (2015). DeCoN: Genome-wide analysis of in vivo transcriptional dynamics during pyramidal neuron fate selection in neocortex. *Neuron* **85**, 275-288. doi:10.1016/j.neuron.2014.12.024

Mulatinho, M., Tenney, J., Vilain, E. and Quintero-Rivera, F. (2016). Microdeletion of ZBTB20 results in a phenotype overlapping with that of the microdeletion 3q13.31 syndrome. *Cancer Genet.* **209**, 244-245. doi:10.1016/j.cancergen.2016.05.050

Nagao, M., Ogata, T., Sawada, Y. and Gotoh, Y. (2016). Zbtb20 promotes astrocytogenesis during neocortical development. *Nat. Commun.* **7**, 11102. doi:10.1038/ncomms11102

O'Leary, D. DM., Ruff, N. L. and Dyck, R. H. (1994). Development, critical period plasticity, and adult reorganizations of mammalian somatosensory systems. *Curr. Opin. Neurobiol.* **4**, 535-544. doi:10.1016/0959-4388(94)90054-X

Raponi, E., Agenes, F., Delphin, C., Assard, N., Baudier, J., Legraverend, C. and Deloulme, J.-C. (2007). S100B expression defines a state in which GFAP-expressing cells lose their neural stem cell potential and acquire a more mature developmental stage. *Glia* **55**, 165-177. doi:10.1002/glia.20445

Rasmussen, M. B., Nielsen, J. V., Lourenço, C. M., Melo, J. B., Halgren, C., Geraldi, C. VL., Marques, W., Jr, Rodrigues, G. R., Thomassen, M., Bak, M. et al. (2014). Neurodevelopmental disorders associated with dosage imbalance of ZBTB20 correlate with the morbidity spectrum of ZBTB20 candidate target genes. *J. Med. Genet.* **51**, 605-613. doi:10.1136/jmedgenet-2014-102535

Rodríguez, C. I., Buchholz, F., Galloway, J., Sequerra, R., Kasper, J., Ayala, R., Stewart, A. F. and Dymecki, S. M. (2000). High-efficiency deleter mice show that FLPe is an alternative to Cre- loxP. *Nat. Genet.* **25**, 139-140. doi:10.1038/75973

Rosenthal, E. H., Tonchev, A. B., Stoykova, A. and Chowdhury, K. (2012). Regulation of archicortical arealization by the transcription factor Zbtb20. *Hippocampus* **22**, 2144-2156. doi:10.1002/hipo.22035

Rowitch, D. H. and Kriegstein, A. R. (2010). Developmental genetics of vertebrate glial-cell specification. *Nature* **468**, 214-222. doi:10.1038/nature09611

Saito, T. and Nakatsuji, N. (2001). Efficient gene transfer into the embryonic mouse brain using in vivo electroporation. *Dev. Biol.* **240**, 237-246. doi:10.1006/dbio.2001.0439

Siggs, O. M. and Beutler, B. (2012). The BTB-ZF transcription factors. *Cell Cycle* **11**, 3358-3369. doi:10.4161/cc.21277

Sun, W., Cornwell, A., Li, J., Peng, S., Joana Osorio, M., Aalling, N., Wang, S., Benraiss, A., Lou, N., Goldman, S. A. et al. (2017). SOX9 is an astrocyte-specific nuclear marker in the adult brain outside the neurogenic regions. *J. Neurosci.* **37**, 4493-4507. doi:10.1523/JNEUROSCI.3199-16.2017

Tang, X., Falls, D. L., Li, X., Lane, T. and Luskin, M. B. (2007). Antigen-retrieval procedure for bromodeoxyuridine immunolabeling with concurrent labeling of nuclear DNA and antigens damaged by HCl pretreatment. *J. Neurosci.* **27**, 5837-5844. doi:10.1523/JNEUROSCI.5048-06.2007

Telley, L., Agirman, G., Prados, J., Amberg, N., Fièvre, S., Oberst, P., Bartolini, G., Vitali, I., Cadilhac, C., Hippenmeyer, S. et al. (2019). Temporal patterning of apical progenitors and their daughter neurons in the developing neocortex. *Science (80-)* **364**, eaav2522. doi:10.1126/science.aav2522

Tonchev, A. B., Tuoc, T. C., Rosenthal, E. H., Studer, M. and Stoykova, A. (2016). Zbtb20 modulates the sequential generation of neuronal layers in developing cortex. *Mol. Brain* **9**, 65. doi:10.1186/s13041-016-0242-2

Wang, F., Flanagan, J., Su, N., Wang, L.-C., Bui, S., Nielson, A., Wu, X., Vo, H.-T., Ma, X.-J. and Luo, Y. (2012). RNAscope: a novel in situ RNA analysis platform for formalin-fixed, paraffin-embedded tissues. *J. Mol. Diagnostics* **14**, 22-29. doi:10.1016/j.jmoldx.2011.08.002

Wise, S. P. and Jones, E. G. (1978). Developmental studies of thalamocortical and commissural connections in the rat somatic sensory cortex. *J. Comp. Neurol.* **178**, 187-208. doi:10.1002/cne.901780202

Woolsey, T. A. and Van der Loos, H. (1970). The structural organization of layer IV in the somatosensory region (S I) of mouse cerebral cortex. The description of a cortical field composed of discrete cytoarchitectonic units. *Brain Res.* **17**, 205-242. doi:10.1016/0006-8993(70)90079-X

Wu, S.-X., Goebbels, S., Nakamura, K., Nakamura, K., Kometani, K., Minato, N., Kaneko, T., Nave, K.-A. and Tamamaki, N. (2005). Pyramidal neurons of upper cortical layers generated by NEX-positive progenitor cells in the subventricular zone. *Proc. Natl. Acad. Sci. USA* **102**, 17172-17177. doi:10.1073/pnas.0508560102

Yu, Y.-C., Bultje, R. S., Wang, X. and Shi, S.-H. (2009). Specific synapses develop preferentially among sister excitatory neurons in the neocortex. *Nature* **458**, 501-504. doi:10.1038/nature07722

DEVELOPMENT